Summer 2020

Network-Based Statistical Analysis of Functional Magnetic Resonance Imaging Data From Aphasia Patients

Xingpei Zhao

Network-based Statistical Analysis of Functional magnetic resonance imaging data from Aphasia patients

by

Xingpei Zhao

Bachelor of Medicine 2013
Anhui Medical University, China

Submitted in Partial Fulfillment of the Requirements

for the Degree of Master of Science in Public Health in

Biostatistics

Arnold School of Public Health

University of South Carolina

2020

Accepted by:

Yuan Wang, Major Professor

Alexander C McLain, Committee Member

Roozbeh Behroozmand, Committee Member

Cheryl L. Addy, Vice Provost and Dean of the Graduate School

Acknowledgments

I would like to express my gratitude to Dr. Yuan Wang, my research advisor, for her patient guidance, professional suggestions and enthusiastic encouragement during all stages of this project. Her willingness to give her time so generously is very much appreciated. Also, her inspiring words boosted my confidence when I faced the difficulties in the academic path. Without her persistent guidance, the goal of this project would not have been achieved.

I would also thank to Dr. Alexander McLain for his help and advice on methodology, and to Dr. Roozbeh Behroozmand for helping me with the interpretation related to language processing. My thanks are also extended to Dr. Lorelei Phillip Johnson and Dr. Grigori Yourganov, as well as the lab members in the Center for the Study of Aphasia Recovery for collecting and preprocessing the dataset used in the thesis.

Finally, I wish to thank my husband, Qingyang Liu, and my parents, Yide Zhao and Changhong Zhang, for their support and encouragement throughout my study.

Abstract

Functional magnetic resonance imaging (fMRI) is a neuroimaging technique that provides insight into brain function and activity. Network models of fMRI signals can reveal functional connectivity related to certain brain disorders, such as post-stroke aphasia. This thesis aims to identify the functional connections that distinguish anomic and Broca's aphasia by comparing the resting-state fMRI from the patients with these two types of aphasia. The network-based statistic (NBS) approach is used to detect such connections. After the analytic pipeline is applied to the fMRI data, the NBS approach identifies a distinct subnetwork between the two types of aphasia, which involves the premotor, primary motor, and prime sensory cortex. By examining the properties of this subnetwork through complex network measures, we found that the regions in the premotor cortex and primary motor cortex play an important role in information flow and overall communication efficiency.

Table of Contents

List of Tables

List of Figures

Chapter 1

Introduction

Neuroimaging is the use of various imaging techniques to visualize the structure, function or pathology of the human brain in vivo. Introduced in the early nineties, functional magnetic resonance image (fMRI) is a safe and non-invasive technique to assess brain function and activity. Exploring a brain from the viewpoint of connectivity patterns reveals important information on the functional organization of the brain [Farahani, Karwowski, and Lighthall, 2019]. To analyze functional connectivity, we can model fMRI data as a network. Nodes in a network represent brain sites or regions of interest (ROIs) and edges are the functional connections between the brain sites or ROIs. When we focus on a specific human behavior or disorder, we want to know whether there exists subnetworks that play a role in it. The network-based statistic (NBS) approach [Zalesky, Fornito, and Bullmore, 2010] provides an efficient process for identifying functional subsets of interest, e.g., subsets of brain regions that distinguish two groups of subjects. The problem of detecting these distinct subsets may involve a massive number of hypothesis tests. Standard mass univariate testing approaches may fail to find significant results or possess sufficient power, whereas the NBS approach potentially provides a higher power by utilizing the presence of connections comprising the subnetwork of interest [Zalesky, Fornito, and Bullmore, 2010]. In this thesis, we want to identify the subset of brain regions or a subnetwork that distinguishes anomic and Broca's aphasia.

1.1 Aphasia

Aphasia is a language impairment that affects a person's ability to read, understand, and speak the language. The causes of aphasia include stroke, tumor, infection, and injury to the brain. Aphasia can be classified into different types based on individual symptoms and location of brain injury. Two common types of aphasia are anomic and Broca's aphasia. Anomic aphasia is a mild, fluent type of aphasia where the patients with anomic aphasia commonly have a problem with word retrieval and cannot express the words they want to say. Their speech fluency, repetition, comprehension, and grammatical speech have been relatively preserved [Dronkers and Baldo, 2009]. On the other hand, Broca's aphasia is a non-fluent type of aphasia. The patients with Broca's aphasia have difficulties in producing language, although their comprehension generally remains intact [Hickok, Bellugi, and Klima, 1998]. They are not able to produce long sentences grammatically and their speech is limited to simple and short utterances. The aphasia type is typically diagnosed through neuroimaging, such as computed tomography (CT) and magnetic resonance imaging (MRI), as well as a series of comprehensive neuropsychological tests.

1.2 Functional magnetic resonance imaging (fMRI)

Functional magnetic resonance imaging or functional MRI (fMRI) is a noninvasive technique that indirectly identifies the neural activity through measuring the blood oxygen level dependent (BOLD) signal. BOLD signal refers to the contrast difference between oxygenated and deoxygenated hemoglobin [Ogawa et al., 1992]. The brain areas that are active during the execution of different tasks consume more oxygen than inactive brain areas. It leads to an increase in the inflow of oxygenated blood to active areas and a decrease in the concentration of deoxyhemoglobin [Lindquist, 2008]. As a result, BOLD signals rise above baseline to a peak level at around $4 \sim 6$

seconds after activation. After the functional activity stops, BOLD signals fall below the baseline level. Over time the BOLD signals recover to the baseline level [Ashby, 2011]. By visualizing fluctuations of BOLD signal, fMRI indirectly shows the extent of neural activity. Resting state fMRI (rs-fMRI) measures BOLD signal when a brain is in a resting state. The rs-fMRI reflects functional brain activities that occur in a default mode.

1.3 Functional connectivity

Functional brain connectivity encompasses the inter-relationships and integrated performance of different brain regions [Rogers et al., 2001]. It can be represented by the correlations of BOLD signals of brain regions [Van den Heuvel and Hulshoff Pol, 2010]. In many cases, we create a network model to analyze functional connectivity. In a functional brain network model, nodes are brain sites or regions of interest (ROIs) and edges are functional connections between these sites or ROIs.

1.4 Thesis motivation and outline

Since the network-based statistic (NBS) approach was first introduced, it has been applied to fMRI data from subjects with schizophrenia [Zalesky, Fornito, and Bullmore, 2010], Alzheimer's Disease [Zhan et al., 2016], Internet addiction [Wen and Hsieh, 2016], and borderline personality disorder [Xu et al., 2016]. In these studies, one or more altered subnetworks that are related to neurological or psychiatric disorders are identified from comparisons between groups of subjects through the NBS approach. In this thesis, we aim to apply the NBS approach to identify a distinctive subnetwork between anomic and Broca's aphasia. Meanwhile, one network analysis method called complex network measures [Rubinov and Sporns, 2010] is used to examine the properties and organization of the distinctive subnetwork between two types of aphasia directly.

The outline of this thesis is as follows:

- In Chapter 2, we introduce the NBS and baseline approaches.
- In Chapter 3, we evaluate the empirical performance of the NBS and baseline approaches under different network sizes and signal-to-noise ratios.
- In Chapter 4, we apply the NBS approach to rs-fMRI data from individuals with anomic and Broca's aphasia. We identify a subnetwork that distinguishes the two types of aphasia.
- In Chapter 5, we discuss the limitations of the NBS and baseline approaches.

Chapter 2

Methods

2.1 Connectivity Matrix

To compare two groups of functional brain networks, we first construct a connectivity matrix from the fMRI data for each subject. The data structure of preprocessed fMRI is

$$\begin{pmatrix} a_{11} & a_{12} & a_{13} & \dots & \dots & a_{1t} \\ a_{21} & a_{22} & a_{23} & \dots & \dots & a_{2t} \\ a_{31} & a_{32} & a_{33} & \dots & \dots & a_{3t} \\ \vdots & \vdots & \vdots & \vdots & \ddots & \vdots \\ a_{N1} & a_{N2} & a_{N3} & \dots & \dots & a_{Nt} \end{pmatrix},$$

where the matrix element a_{ij} represents the BOLD signal at region i and time j, $i = 1, \dots, N$ with N being the number of regions of interest (ROIs) and $j = 1, \dots, t$ with t being the number of time points.

Pearson's correlation coefficients are calculated between the BOLD signals of ROIs. The correlation coefficient r_{ij} between region i and region j is

$$r_{ij} = \frac{\sum_{x=1}^{t} (a_{ix} - \bar{a}_{i\cdot})(a_{jx} - \bar{a}_{j\cdot})}{\sqrt{\sum_{x=1}^{t} (a_{ix} - \bar{a}_{i\cdot})^2} \sqrt{\sum_{x=1}^{t} (a_{jx} - \bar{a}_{j\cdot})^2}} \tag{2.1}$$

where $i, j = 1, \dots, N$ and $i \neq j$. $\bar{a}_{i\cdot}$ and $\bar{a}_{j\cdot}$ are the mean of BOLD signals at region i and region j.

A connectivity matrix of N regions is then

$$\begin{pmatrix} 1 & r_{12} & r_{13} & \dots & \dots & r_{1N} \\ r_{12} & 1 & r_{23} & \dots & \dots & r_{2N} \\ r_{13} & r_{23} & 1 & \dots & \dots & r_{3N} \\ \vdots & \vdots & \vdots & \vdots & \ddots & \vdots \\ r_{1N} & r_{2N} & r_{3N} & \dots & \dots & 1 \end{pmatrix},$$

the entries are correlation coefficients that represent edge weights of the functional connections between the ROIs. Because the connectivity matrix is symmetric, we only study the $N(N-1)/2$ upper triangular or lower triangular entries. The Fisher's z-transformation [Fisher, 1915] is applied to the raw coefficients to insure their normality. The Fisher's z-transformation of r_{ij} is

$$z_{ij} = \frac{1}{2} \ln \left(\frac{1 + r_{ij}}{1 - r_{ij}} \right) = \operatorname{artanh}(r_{ij}) \tag{2.2}$$

where $i, j = 1, \dots, N$ and $i \neq j$.

After a connectivity matrix is established, we construct a binary network through thresholding. There are two methods of thresholding: weight based thresholding and proportional thresholding. Weight based thresholding applies an arbitrary value as a threshold. Only weights that are greater than the threshold are retained and set to 1, whereas the smaller ones (including all negative correlations) are set to 0. As the threshold value increases, edges disappear and the binary network becomes sparser; as the threshold value decreases, edges appear and the binary network becomes denser. Proportional thresholding is to preserve a desired proportion of the largest edges weights and set them to 1.

2.2 Network-based statistic (NBS) approach

We first build a general linear model (GLM) based on the connectivity matrices. The dependent variable $\mathbf{Y}$ is

$$\mathbf{Y} = \begin{bmatrix} \mathbf{y_1} \\ \mathbf{y_2} \\ \vdots \\ \mathbf{y_n} \end{bmatrix},$$

where n is the total number of subjects in two groups and

$$\mathbf{y_i} = (y_{i1}, y_{i2}, y_{i3}, \dots y_{i,(N-1)N/2})^T = (z_{12}, z_{13}, z_{23}, z_{14} \dots z_{N-1,N})^T,$$

which consists of the upper triangular entries in connectivity matrices of subjects i, $i = 1, 2, 3, \dots, n$. The design matrix $\mathbf{X}$ is

$$\mathbf{X} = \begin{bmatrix} 1 & 0 \\ \vdots & \vdots \\ 1 & 0 \\ 0 & 1 \\ \vdots & \vdots \\ 0 & 1 \end{bmatrix},$$

which consists of the group indicators for the subjects and each column represents one of the two groups.

Under this setting, the GLM is

$$\begin{bmatrix} y_{1j} \\ y_{2j} \\ y_{3j} \\ \vdots \\ \vdots \\ y_{nj} \end{bmatrix} = \begin{bmatrix} 1 & 0 \\ \vdots & \vdots \\ 1 & 0 \\ 0 & 1 \\ \vdots & \vdots \\ 0 & 1 \end{bmatrix} \begin{bmatrix} \beta_{1j} \\ \beta_{2j} \end{bmatrix} + \begin{bmatrix} e_{1j} \\ e_{2j} \\ e_{3j} \\ \vdots \\ \vdots \\ e_{nj} \end{bmatrix},$$

where $j = 1, 2, \ldots, N(N-1)/2$ with N being the number of nodes. We assume $e_{\cdot j} \sim MN(0, \Sigma_j)$, $(e_{\cdot j}, e_{\cdot k}), j \neq k$, are uncorrelated with each other and $\Sigma_j = \sigma_j^2 \mathbf{I}$, with $\mathbf{I}$ being the $n \times n$ identity matrix.

The β_{1j} and β_{2j} are the group effects of the normalized correlation coefficients and are estimated by ordinary least-squares estimation:

$$\hat{\boldsymbol{\beta}} = \left(\mathbf{X}^{\mathrm{T}}\mathbf{X}\right)^{-1}\mathbf{X}^{\mathrm{T}}\mathbf{Y},$$

which is equivalent to group sample means of the normalized correlation coefficients. To see this, suppose the number of subjects in Group 1 is n_1, the number of subjects in Group 2 is n_2, and the total number of subjects $n = n_1 + n_2$, then

$$\begin{aligned}(\mathbf{X}^T\mathbf{X})^{-1} &= \left(\begin{bmatrix} 1 & \ldots & 1 & 0 & \ldots & 0 \\ 0 & \ldots & 0 & 1 & \ldots & 1 \end{bmatrix} \begin{bmatrix} 1 & 0 \\ \vdots & \vdots \\ 1 & 0 \\ 0 & 1 \\ \vdots & \vdots \\ 0 & 1 \end{bmatrix} \right)^{-1} \\ &= \left(\begin{bmatrix} n_1 & 0 \\ 0 & n_2 \end{bmatrix} \right)^{-1} = \begin{bmatrix} \frac{1}{n_1} & 0 \\ 0 & \frac{1}{n_2} \end{bmatrix},\end{aligned}$$

$$\begin{aligned}\mathbf{X}^T\mathbf{Y} &= \begin{bmatrix} 1 & \ldots & 1 & 0 & \ldots & 0 \\ 0 & \ldots & 0 & 1 & \ldots & 1 \end{bmatrix} \begin{bmatrix} y_{11} & \cdots & y_{1,N(N-1)/2} \\ y_{21} & \cdots & y_{2,N(N-1)/2} \\ \vdots & \vdots & \vdots \\ y_{n_1,1} & \cdots & y_{n_1,N(N-1)/2} \\ \vdots & \vdots & \vdots \\ y_{n_1+n_2,1} & \cdots & y_{n_1+n_2,N(N-1)/2} \end{bmatrix} \\ &= \begin{bmatrix} \sum_{i=1}^{n_1} y_{i1} & \cdots & \sum_{i=1}^{n_1} y_{i,N(N-1)/2} \\ \sum_{i=n_1+1}^{n_1+n_2} y_{i1} & \cdots & \sum_{i=n_1+1}^{n_1+n_2} y_{i,N(N-1)/2} \end{bmatrix}.\end{aligned}$$

Therefore,

$$\begin{aligned}\hat{\beta} &= (\mathbf{X}^T\mathbf{X})^{-1}\mathbf{X}^T\mathbf{Y} \\ &= \begin{bmatrix} \frac{1}{n_1} & 0 \\ 0 & \frac{1}{n_2} \end{bmatrix} \begin{bmatrix} \sum_{i=1}^{n_1} y_{i1} & \cdots & \sum_{i=1}^{n_1} y_{i,N(N-1)/2} \\ \sum_{i=n_1+1}^{n_1+n_2} y_{i1} & \cdots & \sum_{i=n_1+1}^{n_1+n_2} y_{i,N(N-1)/2} \end{bmatrix} \\ &= \begin{bmatrix} \frac{\sum_{i=1}^{n_1} y_{i1}}{n_1} & \cdots & \frac{\sum_{i=1}^{n_1} y_{i,N(N-1)/2}}{n_1} \\ \frac{\sum_{i=n_1+1}^{n_1+n_2} y_{i1}}{n_2} & \cdots & \frac{\sum_{i=n_1+1}^{n_1+n_2} y_{i,N(N-1)/2}}{n_2} \end{bmatrix},\end{aligned}$$

which are the group sample means for the normalized correlation coefficients.

On the other hand, the σ_j^2 is estimated by adjusted sum of squared residuals, where the residuals are defined as $\mathbf{Y} - \mathbf{X}\hat{\beta}$ and squared residuals are computed by

$$(\mathbf{Y} - \mathbf{X}\hat{\beta}) \circ (\mathbf{Y} - \mathbf{X}\hat{\beta})$$

where $\circ$ is the Hadamard product or element-wise product. Therefore,

$$\hat{\sigma}_j^2 = \frac{1}{n_1 + n_2 - 2}\left[\left(y_{1j} - \frac{\sum_{i=1}^{n_1} y_{ij}}{n_1}\right)^2 + \cdots + \left(y_{n_1+n_2,j} - \frac{\sum_{i=n_1+1}^{n_1+n_2} y_{ij}}{n_2}\right)^2\right].$$

We are interested in the differences in the correlation coefficients of the two groups. Under the null hypothesis, we assume no difference in the correlation coefficients of two groups, i.e.

$$H_0 : \beta_{1j} = \beta_{2j}, j = 1, 2, \ldots, N(N-1)/2.$$

With the contrast vector $\mathbf{L} = [1 \; -1]$, the test statistic at j^{th} comparison can be computed by

$$T_j = \frac{\mathbf{L}\hat{\beta}_{\cdot j}}{\sqrt{\hat{\sigma}_j^2 \mathbf{L}(\mathbf{X}^T\mathbf{X})^{-1}\mathbf{L}^T}}. \tag{2.3}$$

In total, $N(N-1)/2$ test statistics are computed as weighted group differences in normalized correlation coefficients.

The next step is to obtain suprathreshold edges by thresholding. After a threshold is selected, if the test statistic with a value greater than the threshold, an edge weight associated with it is set to 1; otherwise, 0. The edge surviving thresholding are called

suprathreshold edges. By doing this, we construct an adjacency matrix and preserve initial positions of edge weights in the connectivity matrix. In the adjacency matrix, the 1s indicate suprathreshold edges or large group differences declared significant. The NBS seeks to identify any potentially connected structures formed by the set of suprathreshold edges in the adjacency matrix [Zalesky, Fornito, and Bullmore, 2010]. The algorithm, called breadth first search [Ahuja et al., 1993], is used to identify any connected structure(s) or component(s). The maximum number of edges that make up each component is defined as the size S for observed connected component. Among each connected component, there exists a suprathreshold edge between any paired nodes.

There are two ways to measure the size of a connected component. One way is by counting the total number of suprathreshold edges (non-zero elements) in a connected component. It is called component extent. Another way is by computing the sum of test statistics values across all edges in a component. It is called component intensity. According to Zalesky, Fornito, and Bullmore (2010), component extent is suited to detecting a relative week connections, while component intensity is suited a strong, focal effect confined to relatively few connections.

We then conduct a permutation test based on the test statistics and assumption of group exchangeability. During each permutation, the subjects from two groups are mixed up and then pooled subjects are divided into two groups randomly. New test statistics of all comparisons are computed again based on the new grouping. The same threshold applied to the observed test statistic is applied to the new test statistic and construct a new adjacency matrix. After applying the threshold, the maximum component(s) size S^* is determined. After M permutations, the p-value for an identified component is estimated by $\hat{p} = P(S^* \geq S)$.

2.3 Complex network measures

After a distinctive network component is identified, complex network measures can be used to characterize the subnetwork.

Let D be the set of all nodes in a network, N be the number of nodes, L be the set of all edges in a network, l be number of edges, (i, j) be an edge between nodes i and j, $(i, j \in D)$, a_{ij} be the connection status between node i and node j. For a binary undirected network,

$$a_{ij} = \begin{cases} 1, \text{when there is a connection between node } i \text{ and node } j \\ 0, \text{ otherwise.} \end{cases}$$

Degree is the number of edges connected to node i,

$$k_i = \sum_{j \in D} a_{ij}. \tag{2.4}$$

Triangles is a set of three nodes, where each node has a edge connected to all other nodes. Given node i, the number of triangles around it,

$$t_i = \frac{1}{2} \sum_{j,h \in D} a_{ij} a_{ih} a_{jh}. \tag{2.5}$$

A shortest path in a binary network is a path with the minimum numbers of edges between two nodes. The length of a shortest path or distance between node i and node j is

$$d_{ij} = \sum_{a_{uv} \in g_{i \leftrightarrow j}} a_{uv} \tag{2.6}$$

where $g_{i \leftrightarrow j}$ is the shortest path between node i and node j. Note that $d_{ij} = \infty$ for all disconnected pairs i,j.

Functional segregation in a brain network is the ability for specialized processing to occur within densely interconnected groups of brain regions [Rubinov and Sporns, 2010]. One basic measure of functional segregation is based on the number of triangles at a given node. A node with a large number of triangles implies there is segregation.

Another common measure of segregation, which is called clustering coefficient, is studied in this thesis. It is the fraction of triangles around a given node [Watts and Strogatz, 1998]. The clustering coefficient of node i,

$$C_i = \begin{cases} \frac{2t_i}{k_i(k_i-1)}, k_i \geq 2 \\ 0, k_i < 2. \end{cases} \tag{2.7}$$

In the Figure 2.1, the clustering coefficient of three red dots are 0, 0.5 and 1.

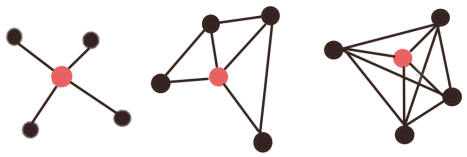

Figure 2.1: Example: clustering coefficient

Hubs in a brain network often play an important role in brain communication and integration [Van den Heuvel and Sporns, 2013]. The basic measure, degrees, can be treated as a simple measure of centrality. The larger the degree, the more central the node is. Another more sensitive measure of centrality is betweenness centrality, which is based on the shortest path. Betweenness centrality is the fraction of all shortest paths in the network pass through a given node. Similar to the degrees, the node with a high betweenness centrality is regarded as a bridge that connects with other nodes in a network. If the nodes with large betweenness centrality are removed, it would cause parts of the network become disconnected.

The betweenness centrality of node i is

$$b_i = \frac{1}{(N-1)(N-2)} \sum_{\substack{h,j=D \\ n\neq j, h\neq j\neq i}} \frac{\rho_{hj}(i)}{\rho_{hj}} \tag{2.8}$$

where ρ_{hj} is the number of shortest paths between nodes h and j, and $\rho_{hj}(i)$ is the number of shortest paths between h and j that pass through node i. The part $\frac{1}{(N-1)(N-2)}$ is used to normalize raw fraction [Freeman, 1977]. The example of betweenness centrality in a network before normalization is shown in Figure 2.2 [Meghanathan, 2016], where the number in a node is betweenness centrality value.

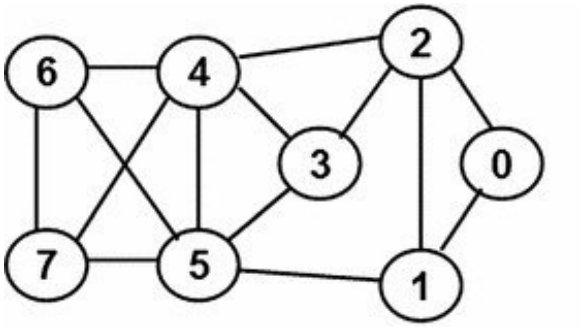

Figure 2.2: Example: betweenness centrality

2.4 Baseline approaches

To compare with the NBS approach, baseline approaches are applied. After test statistics are computed on the $N(N-1)/2$ normalized correlation coefficients between paired regions, multiple comparison corrections are applied to correct multiple p-values and to control the family-wise error rate (FWER). We then use permutation test to estimate the null distribution of $N(N-1)/2$ test statistics. During the M permutations, test statistics are obtained from Equation 2.3. The p-value of test statistic T_j^* is estimated by $\hat{p}_j = P(T_j^* \geq T_j)$, given that the null hypothesis is true.

2.4.1 Bonferroni correction

The most commonly used multiple comparison correction is the Bonferroni correction [Bonferroni, 1936]. By the Bonferroni correction, the null hypothesis is rejected for each $p_j \leq \frac{\alpha}{N(N-1)/2}$, where α is the significant level in $(0, 1)$. The proof of controlling the FWER at α by the Bonferroni correction is in Appendix A. But the

Bonferroni correction is too conservative. If we have a massive number of tests, then we may fail to find any significant results after the Bonferroni correction.

2.4.2 Holm's Bonferroni correction

An improved correction approach is the Holm's Bonferroni correction [Holm, 1979]. The steps of the Holm's Bonferroni correction are: 1) let $H^1, \ldots, H^m$ be a set of null hypotheses and let $p_1, \ldots, p_m$ be the corresponding p-values, where $m = N(N-1)/2$; 2) sort the p-values from the lowest to the highest $p_{(1)}, \ldots, p_{(m)}$ and let the associated hypotheses be $H^{(1)}, \ldots, H^{(m)}$; 3) for a given significance level α, let k be the minimal index such that $p_{(k)} > \frac{\alpha}{m+1-k}$. Then we reject the null hypotheses $H^{(1)}, \ldots, H^{(k-1)}$ and do not reject $H^{(k)}, \ldots, H^{(m)}$. The Holm's Bonferroni correction ensures that the FWER is less than α (Appendix A).

2.4.3 FDR control

The false discovery rate (FDR) is another procedure for controlling Type I errors when performing multiple comparisons. Compared with the Bonferroni and the Holm's Bonferroni correction, FDR control is less stringent at the cost of increasing Type I errors. The purpose of FDR is to control the expected proportion of discoveries (null hypotheses which are declaring significant) that are incorrect [Benjamini and Hochberg, 1995]. The method used in this thesis is the Benjamini–Hochberg procedure, also known as the BH step-up procedure. Suppose the BH step-up procedure controls the FDR at level q and m tests are performed, where $m = N(N-1)/2$, the first step is sorting all the p-values from the smallest to the largest as: $p_{(1)}, p_{(2)}, p_{(3)}, \ldots, p_{(m)}$. If the largest k such that $p_{(k)} \leq \frac{k}{m}q$, we reject the null hypotheses for $H^{(1)}, \ldots, H^{(k)}$. The proof of the FDR control is in Appendix A.

Chapter 3

Simulation Studies

The probability of making at least one Type I error, or finding at least one false positive in the multiple tests, is defined as the family-wise error rate (FWER). When we test a massive number of hypotheses in network comparison, the FWER increases dramatically. To control the FWER given a significant level, we perform the NBS and baseline approaches with multiple comparison corrections (Bonferroni, Holm's Bonferroni, and FDR). The purpose of these simulation studies is to evaluate the empirical performance of the NBS approach against the baseline approaches.

The performance of approaches is evaluated by their true positive rate (TPR) and false positive rate (FPR). Under the null hypotheses, we assume no differences in edge weights between two groups of networks. Suppose P is the set of edges that differ between the two groups, R is the set of edges that do not differ between the groups, and $\hat{h}$ is the set of edges that make up the component or the set of edges declared significant by the NBS and baseline approaches. Then, the TPR is defined as $|P \cap \hat{h}|/|P|$ and the FPR is defined as $|R \cap \hat{h}|/|R|$.

3.1 Simulations

We first generate two groups of networks that do not differ. The groups sizes of Group 1 and Group 2 are n_1 and n_2. The edge weight z_{ij} in a network is generated from the Gaussian distribution with mean $= arctanh(r_{ij})$ and standard deviation $= 1/\sqrt{N(N-1)/2-3}$, where r_{ij} follows an uniform distribution with $(-1, 1)$, $i, j = 1, 2, \ldots, N$ with N being the number of nodes in a network.

Then, we assign the edges with weights that differ between the two groups to the networks in Group 2. To generate these edges, a symmetric adjacency matrix is generated from the Erdős–Rényi random graph model [Erdős and Rényi, 1960] with N and c_r, where c_r is the probability that an edges exists between any two distinct nodes. The existence of each edge is independent of other edges. After that, the diagonal elements in the matrix are set to 0. The number of non-zero elements in the adjacency matrix is approximately equal to $N \times N \times c_r$. The non-zero elements represents the edges with weights that differ between the two groups. Signal-to-noise ratio (SNR), which is the ratio of the number of the edges with distinctive weights to the number of total edges, is approximately equal to c_r. The weights that differ two groups are generated from the Gaussian distribution with mean 0.03 and standard deviation 0.1. Figure 3.1 shows an example of networks from Group 1 and Group 2 with $N = 20$ and $c_r = 0.1$. Figure 3.2 shows the edges with the weights that differ two groups with $c_r = 0.1$.

We consider three simulation studies:

Study 1: We generate two groups of 20×20 networks with group size $n_1 = n_2 = 10$. Around 10% of edges, i.e. 20 edges, in the networks of Group 2 contains weights that differ from Group 1. The SNR is $20/190 \approx 0.1 = c_r$.

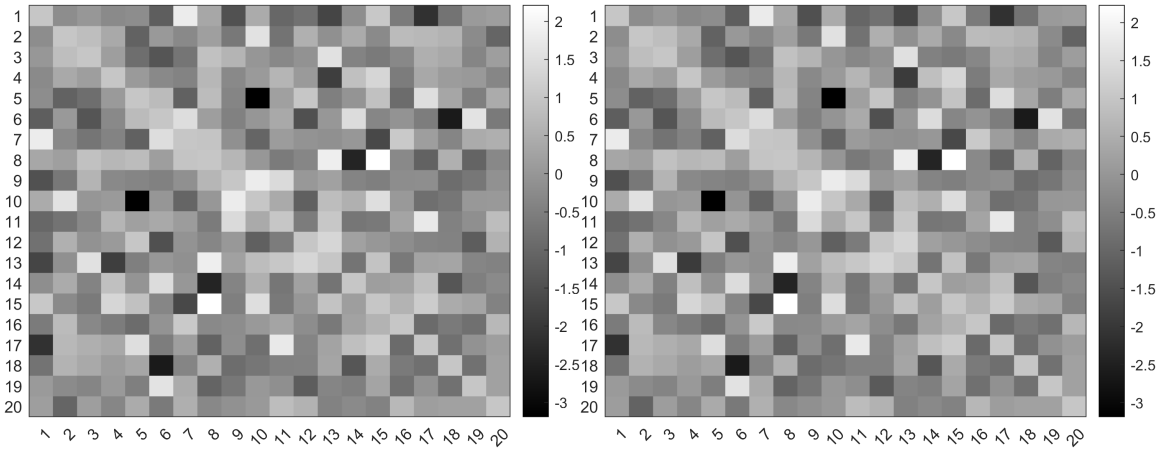

Figure 3.1: Networks from Group 1 and Group 2 with $N = 20$ and c_r=0.1

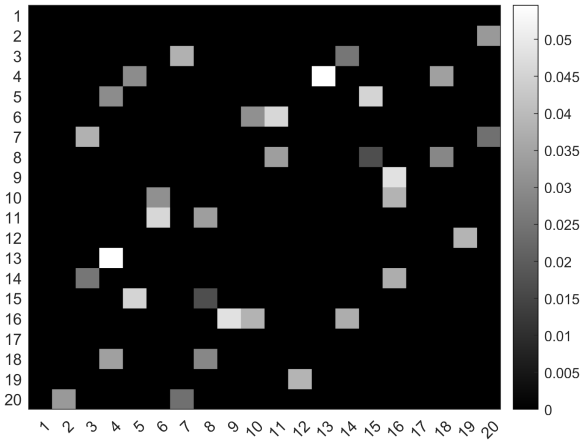

Figure 3.2: Edges with distinct weights, $N = 20$ and c_r=0.1

Study 2: We generate two groups of 40×40 networks with group size $n_1 = n_2 = 10$. Around 10% of edges, i.e. 80 edges, in the networks of Group 2 contains weights that differ from Group 1. The SNR is $80/780 \approx 0.1 = c_r$. We consider the same SNR but different network size in this study.

Study 3: We generate two groups of 40×40 networks with group size $n_1 = n_2 = 10$. Around 5% of edges, i.e. 40 edges, in the networks of Group 2 contains weights that differ from Group 1. The SNR is $40/780 \approx 0.05 = c_r$. We consider the same network size but different SNR in this study.

The steps of the simulation studies are as follows:

i Generate two groups of $N \times N$ networks with group size $n_1 = n_2 = 10$, where $N = 20$ in Study 1, $N = 40$ in Study 2 and Study 3. Approximately $100c_r$% of edges in the networks of Group 2 contain the weight that differ between two groups, where $c_r = 0.1$ in Study 1 and Study 2, $c_r = 0.05$ in Study 3.

ii Construct hypothesis tests from the GLM for detecting group differences. Then compute test statistics.

iii Perform the NBS with the threshold 2.5 and baseline approaches to identify subnetwork or the set of edges that differ significantly between two groups.

The significant level and q level that are used in the simulation studies are 0.05. The total number of permutations is $5,000$.

iv Compare the identified subnetwork or the set of edges that differ significantly between the two groups to the edges contains distinctive weights.

v Iterate 2,000 and 5,000 times. Then compute the TPR and the FPR of the NBS and baseline approaches respectively.

3.2 Results

Study 1: $N = 20, c_r = 0.1$**.** Figure 3.3 shows the edges with weights that differ between the two groups. Figure 3.4 shows the subnetwork that is identified by the NBS with threshold 2.5. Figure 3.5, 3.6 and 3.7 show the edges that are declared significant by baseline approaches with different multiple comparison corrections. Table 3.1 lists the average TPR and FPR of the NBS approach and baseline approaches after 5,000 simulations.

We find that the Bonferroni and Holm's Bonferroni corrections are too conservative to detect differences. Only parts of edges with distinctive weights are detected by the Bonferroni and Holm's Bonferroni correction. The ability to detecting group dif-

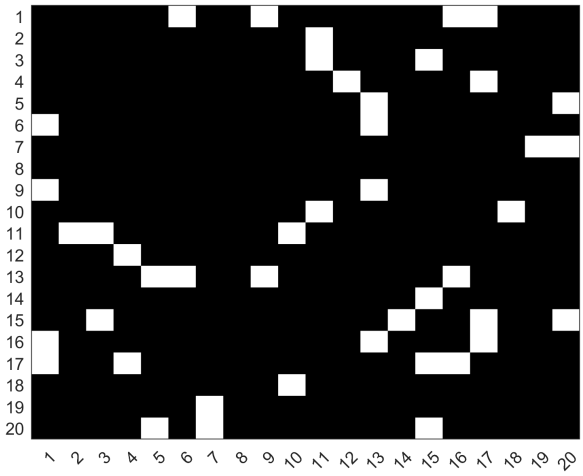

Figure 3.3: Edges with distinctive weights in Study 1 (N=20, c_r=0.1)

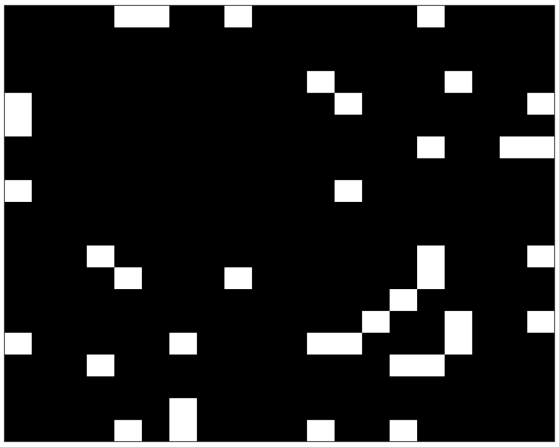

Figure 3.4: NBS

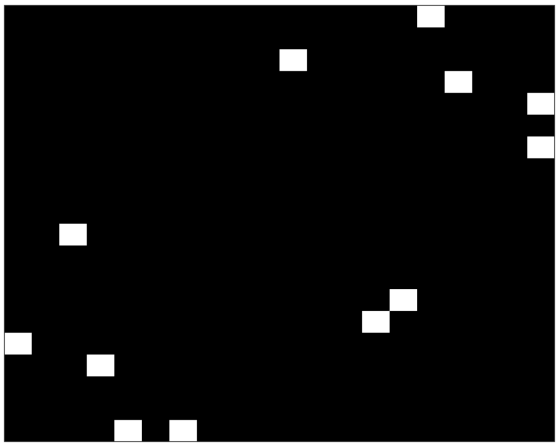

Figure 3.5: Bonferroni correction

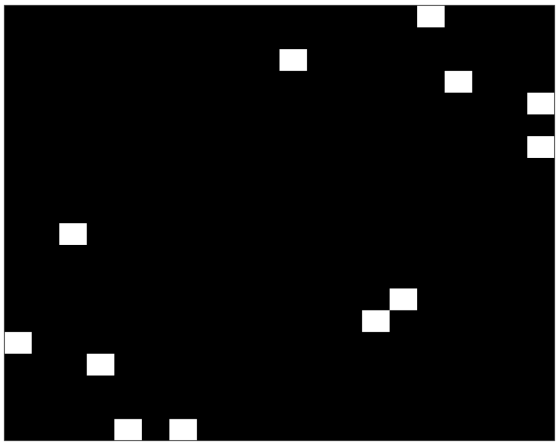

Figure 3.6: Holm's Bonferroni

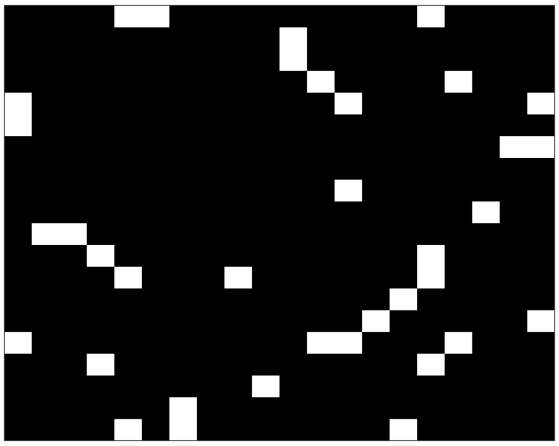

Figure 3.7: FDR

Table 3.1: The average TPR and FPR for the networks with N=20, c_r=0.1, after 5,000 simulations

	NBS	**Bonferroni**	**Holm's Bonferroni**	**FDR**
TPR	0.72776250	0.25383687	0.25383687	0.58956368
FPR	0.00892555	0.00017368	0.00017368	0.00157572

ferences for the FDR and the NBS approach are better, compared with the Bonferroni and Holm's Bonferroni corrections. Most edges with distinctive weights are identified by the FDR and the NBS approach. From the results of average TPR and FPR, we find that the NBS approach is able to detect small differences by scarifying its accuracy. The baseline approach with FDR performs well, compared with Bonferroni correction and Holm's Bonferroni correction. The FPR of FDR is desirable.

Study 2: $N = 40, c_r = 0.1$**.** Figure 3.8 shows the edges with weights that differ between the two groups. Figure 3.9 shows the subnetwork that is identified by the NBS with the threshold 2.5. Figure 3.10, 3.11 and 3.12 show the the set of edges that is declared significant by baseline approaches. Table 3.2 lists the average TPR and FPR after 5,000 simulations.

When the network size increases, we find that the average TPR for the NBS and baseline approaches both increase. The NBS approach with the threshold 2.5 has the largest TPR and FPR. The baseline approach with FDR detects a desirable proportion of contrast edges and contains a small number of false discoveries.

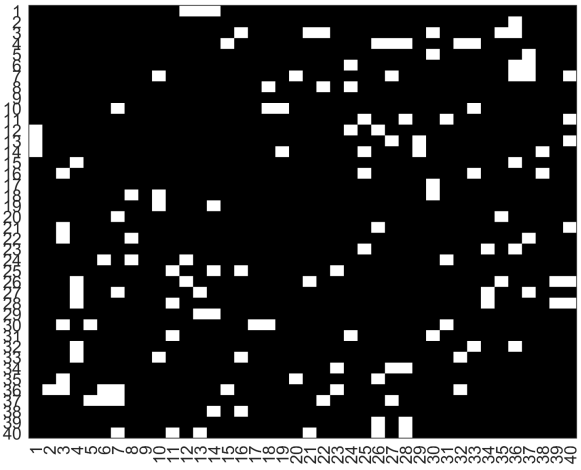

Figure 3.8: Edges with distinctive weights in Study 2 ($N = 40, c_r = 0.1$)

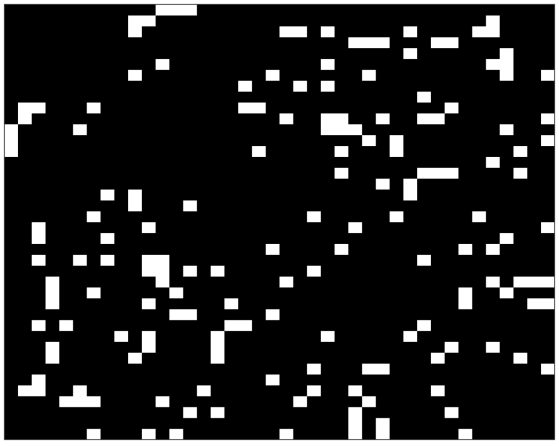

Figure 3.9: NBS

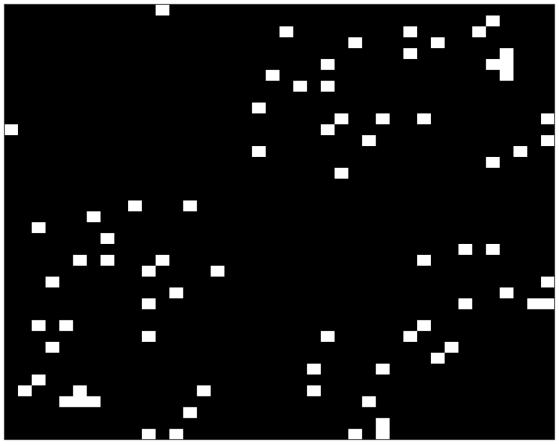

Figure 3.10: Bonferroni correction

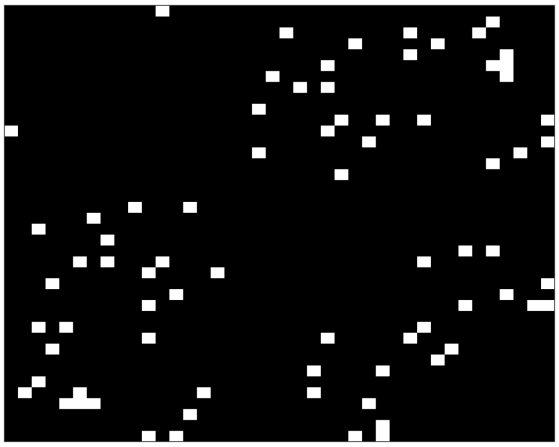

Figure 3.11: Holm's Bonferroni

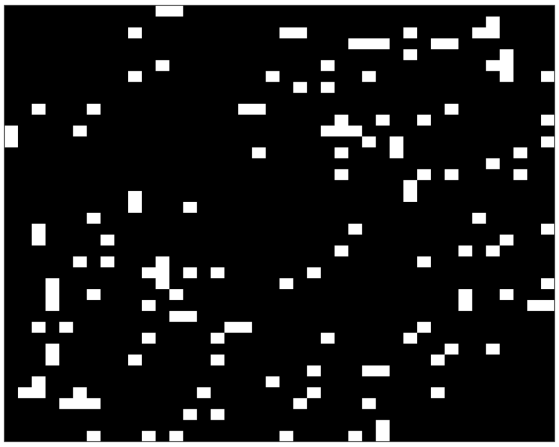

Figure 3.12: FDR

Table 3.2: TPR and FPR for the networks with N=40 and c_r=0.1, after 5,000 simulations

	NBS	**Bonferroni**	**Holm's Bonferroni**	**FDR**
TPR	0.95568855	0.56701087	0.56701087	0.94312512
FPR	0.01030752	0.00009079	0.00009079	0.00235737

Study 3: $N = 40, c_r = 0.05$**.** Figures 3.13 shows the edges with weights that differ the between two groups. Figure 3.14 shows the subnetwork that is identified by the NBS with the threshold 2.5. Figure 3.15, 3.16 and 3.17 show the set of edges that is declared significant by baseline approaches. Table 3.3 lists the average TPR and FPR after 5,000 simulations.

The characteristics of the NBS and baseline approaches shown in this study are similar as the previous ones. When network size is constant and the SNR is decreasing, the TPR of the NBS approach and the baseline approach with FDR decrease, but are still preferable. The TPR of Bonferroni and Holm's Bonferroni corrections are stable. The FPR of the NBS and baseline approaches with the Bonferroni and Holm's Bonferroni correction do not change. The FPR of FDR decreases.

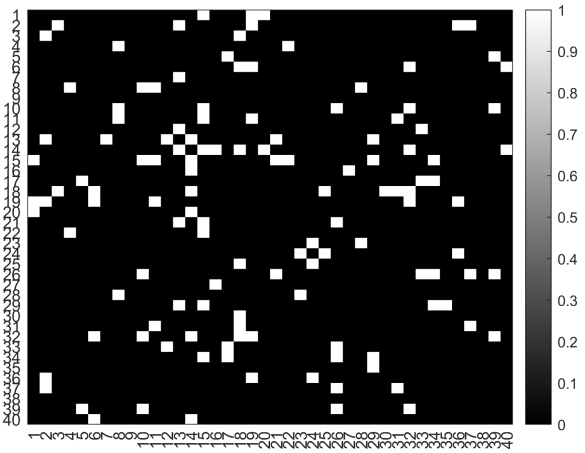

Figure 3.13: Edges with distinctive weights in Study 3($N = 40, c_r = 0.05$)

Figure 3.14: NBS

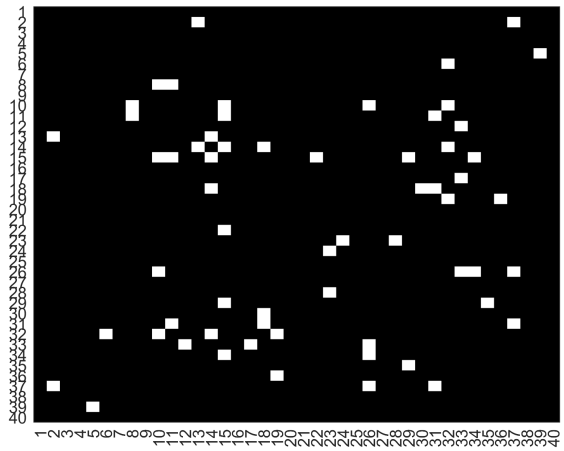

Figure 3.15: Bonferroni correction

Figure 3.16: Holm's Bonferroni

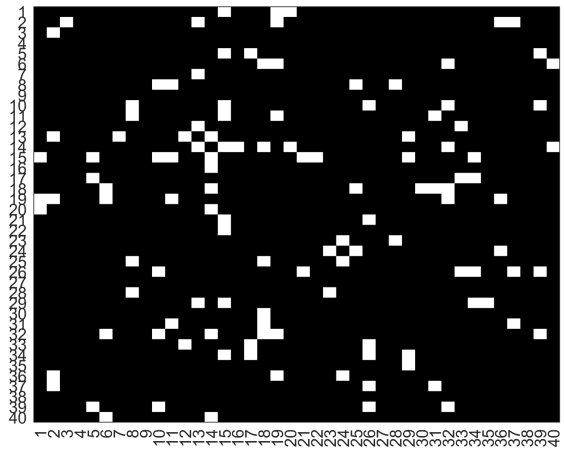

Figure 3.17: FDR

Table 3.3: TPR and FPR for the networks with N=40 and c_r=0.05, after 5,000 simulations

	NBS	**Bonferroni**	**Holm's Bonferroni**	**FDR**
TPR	0.93170053	0.56870990	0.56870990	0.92697352
FPR	0.01039652	0.00009083	0.00009083	0.00124387

In summary, from the results of simulation studies, we learn that the NBS approach detects small group differences well under various network sizes and the SNRs by scarifying its accuracy, compared with baseline approaches. Under the baseline approaches, the FDR has the highest power and desirable FPR. The baseline approaches with Bonferroni and Holm's Bonferroni corrections are very conservative to identify contrast edges.

Chapter 4

Data application

In this chapter, the network-based statistic (NBS) and baseline approaches are going to be applied to the resting-state fMRI (rs-fMIR) data from 48 individuals with anomic ahd Broca's aphasia. The aim of the analysis is to identify the subnetwork that distinguishes anomic and Broca's aphasia and to study properties of this subnetwork through complex network measures.

4.1 Data

The rs-fMRI data were acquired on a Siemens Prisma 3T scanner with a 20-channel head coil located at the Center for the Study of Aphasia Recovery at the University of South Carolina (UofSC). All 48 participants were recruited from the local community as part of a study of post-stroke aphasia. The research was approved by the Institutional Review Board at the UofSC. Among the 48 participants, 14 were diagnosed with the anomic aphasia and 34 were diagnosed with Broca's aphasia. The mean age in anomic aphasia group is 62.70 years old and the mean age in Broca's apahsia group is 59.82 years old; 57% of the participants in anomic aphasia group are male and 67% of Broca's aphasia group are male. The mean score of revised Western Aphasia Battery (WAB-r), a quantitative measurement of the severity of language impairment [Kertesz and Poole, 2004], is 86.79 for anomic aphasia group, and 46.44 for the Broca's aphasia group.

During the scanning process, the participants were instructed to stay still with eyes closed. The following imaging parameters of images were used: a multiband

sequence (x2) with a 216×216 mm field of view, a 90×90 matrix size, and a 72-degree flip angle, 50 axial slices (2 mm thick with 20% gap yielding 2.4 mm between slice centers), repetition time (TR) of 1650 ms, TE=35 ms, GRAPPA=2, 44 reference lines, interleaved ascending slice order [Yourganov et al., 2017]. A total of 370 volumes were acquired. The pre-processing procedures of the fMRI data include motion correction, brain extraction and time correction. During brain extraction, data were extracted from voxels and created 384 regions of interest (ROIs) by AICHA atlas [Joliot et al., 2015].

4.2 Data analysis

4.2.1 Analysis on both hemispheres

A 384×384 connectivity matrix is constructed for each participant. Figure 4.1 shows one connectivity matrix from two aphasia groups. Both raw correlation coefficients and normalized coefficients are presented.

The two groups of normalized correlation coefficients are modeled by the GLM, as follows

$$\begin{bmatrix} y_{1j} \\ y_{2j} \\ \vdots \\ y_{15,j} \\ y_{16,j} \\ \vdots \\ y_{48,j} \end{bmatrix} = \begin{bmatrix} 1 & 0 \\ 1 & 0 \\ \vdots & \vdots \\ 0 & 1 \\ 0 & 1 \\ \vdots & \vdots \\ 0 & 1 \end{bmatrix} \begin{bmatrix} \beta_{1,j} \\ \beta_{2,j} \end{bmatrix} + \begin{bmatrix} e_{1j} \\ e_{2j} \\ \vdots \\ e_{15,j} \\ e_{16,j} \\ \vdots \\ e_{48,j} \end{bmatrix},$$

with $j = 1, 2 \ldots 73,536$. Under the null hypothesis of the analysis, we assume no difference in correlation coefficients between anomic and Brcoa's aphasia groups, i.e.

$$H_0 : \beta_{1,j} = \beta_{2,j}, j = 1, 2, \ldots, 73,536.$$

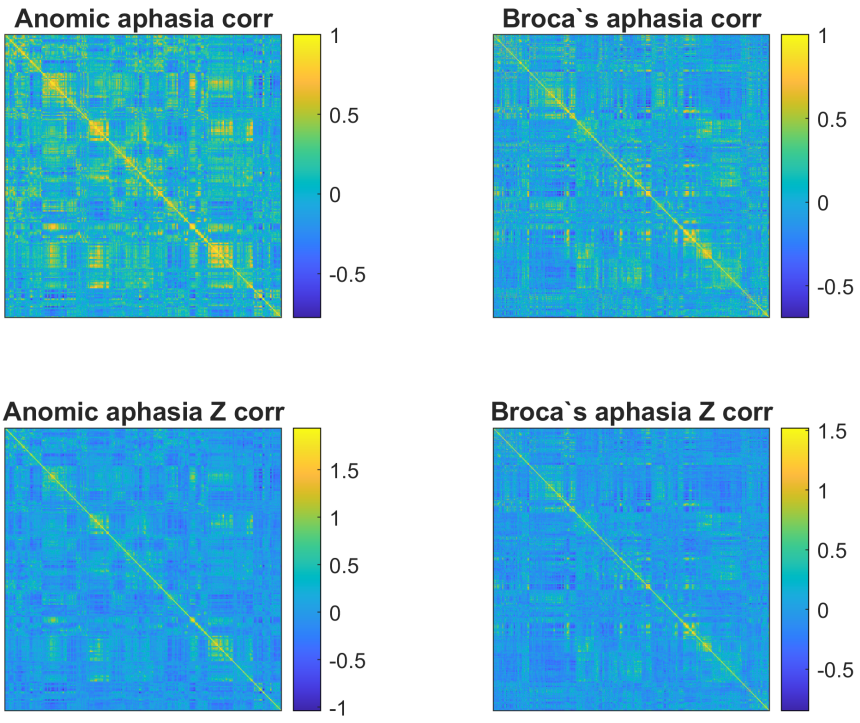

Figure 4.1: Connectivity matrices from anomic and Broca's aphasia group

The test statistics are computed by the equation 2.3. The NBS approach with different thresholds is applied in the analysis. To serve as a comparison, baseline approaches are performed. The FWER and FDR are controlled at 0.05. The total number of permutations is 5,000.

The adjacency matrices present in Figure 4.2 show the subnetworks identified by the NBS with the threshold $3.0, 3.5, 4.0$ and 4.5, which distinguish the anomic aphasia and Broca's aphasia. When the threshold is greater, the size of identified subnetwork is smaller. The detailed figures with ROI labels are presented in Figure B.1, B.2, B.3 and B.4 in Appendix B. The adjacency matrices present in Figure 4.3 show the edges identified by baseline approaches and the subnetwork identified by the NBS with threshold 3.0. When the threshold of the NBS approach increases to 4.0, the result tends to be similar with the results from baseline approaches. When the threshold is between 3.0 and 4.0, the NBS detects more small differences than baseline approaches.

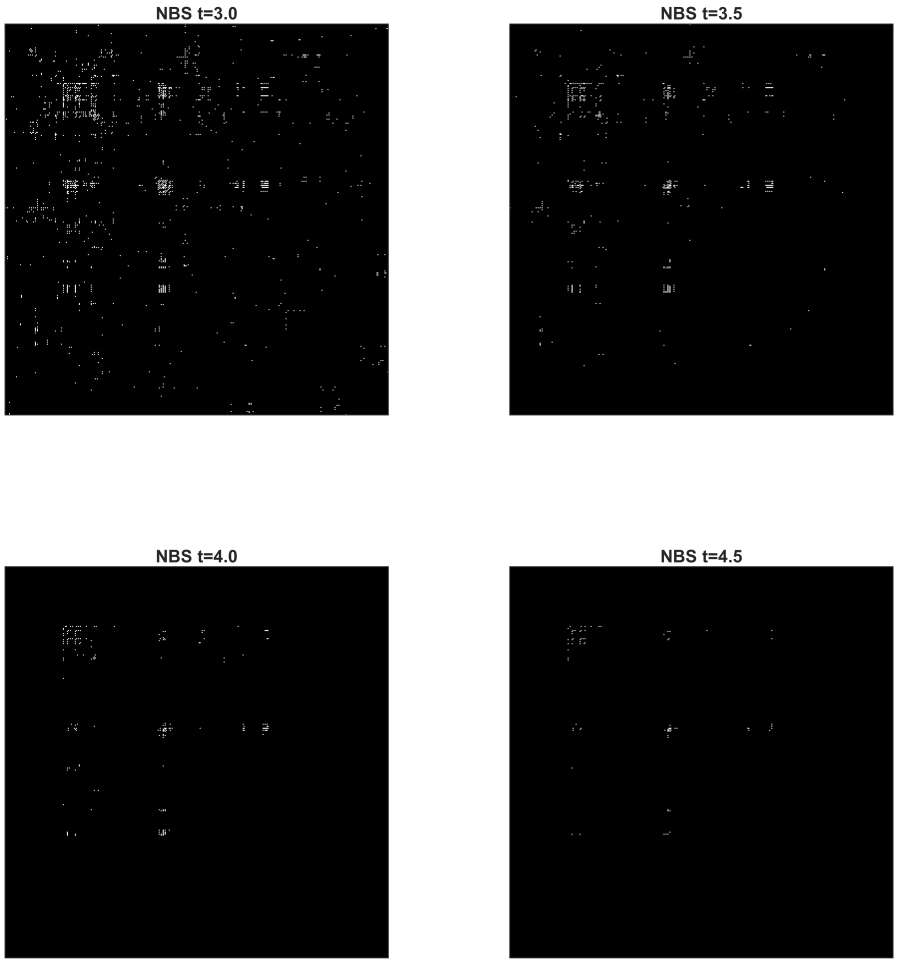

Figure 4.2: Adjacency matrices showing subnetworks identified by the NBS approach with different thresholds

Figure 4.4 shows the subnetwork identified by the NBS with threshold 4.0 from sagittal plane, axial plane and coronal plane of a brain [Xia, Wang, and He, 2013]. The distinctive subnetwork mainly involves ROIs in the premotor, primary motor, primary auditory, and primary sensory cortex of both hemispheres. A few nodes exist in the Broca's area and cingulate cortex of left hemisphere. These areas are involved in the auditory system and motor system, which are responsible for production of and perception of speech [Hickok, Houde, and Rong, 2011]. Table B.1 in Appendix

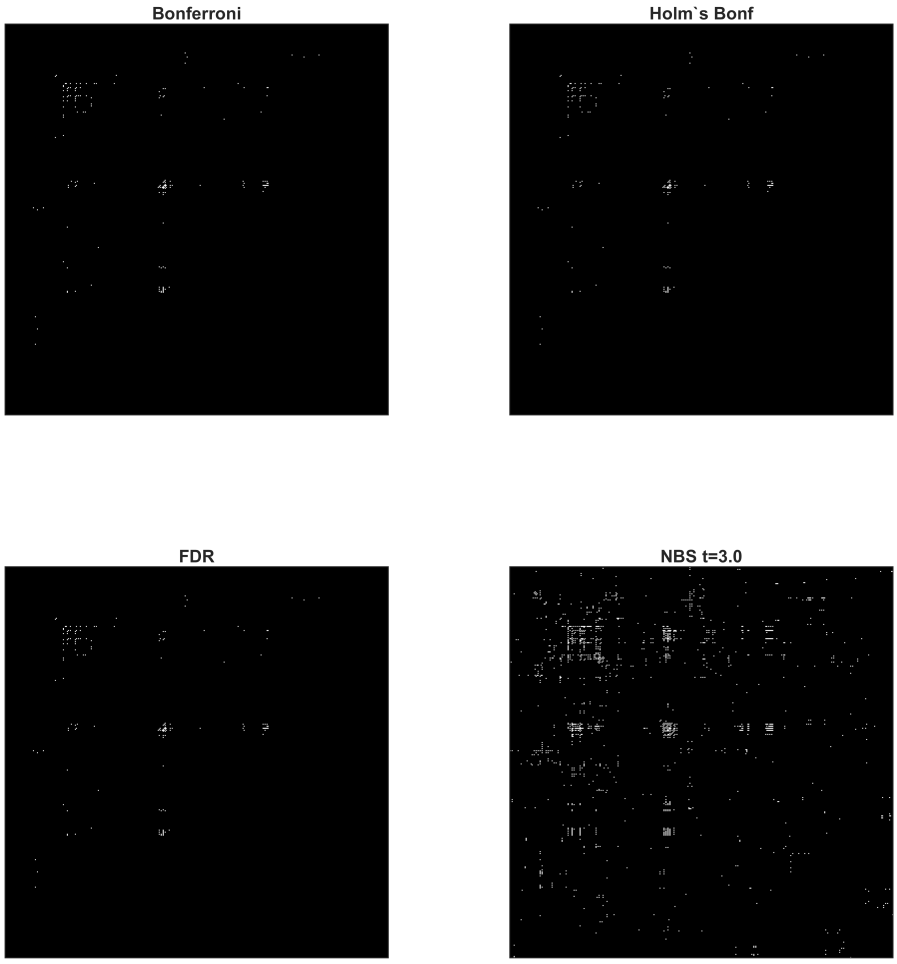

Figure 4.3: Adjacency matrices showing the subnetwork or distinctive edges identified by the NBS and baseline approaches

B lists the nodes making up the distinctive subnetwork as well as their Montreal Neurological Institute (MNI) brain coordinates [Joliot et al., 2015].

4.2.2 Analysis on left hemisphere

If we focus on the ROIs on the left hemisphere, the null hypotheses are

$$H_0 : \beta_{1,j} = \beta_{2,j}, j = 1, 2, ..., 18336.$$

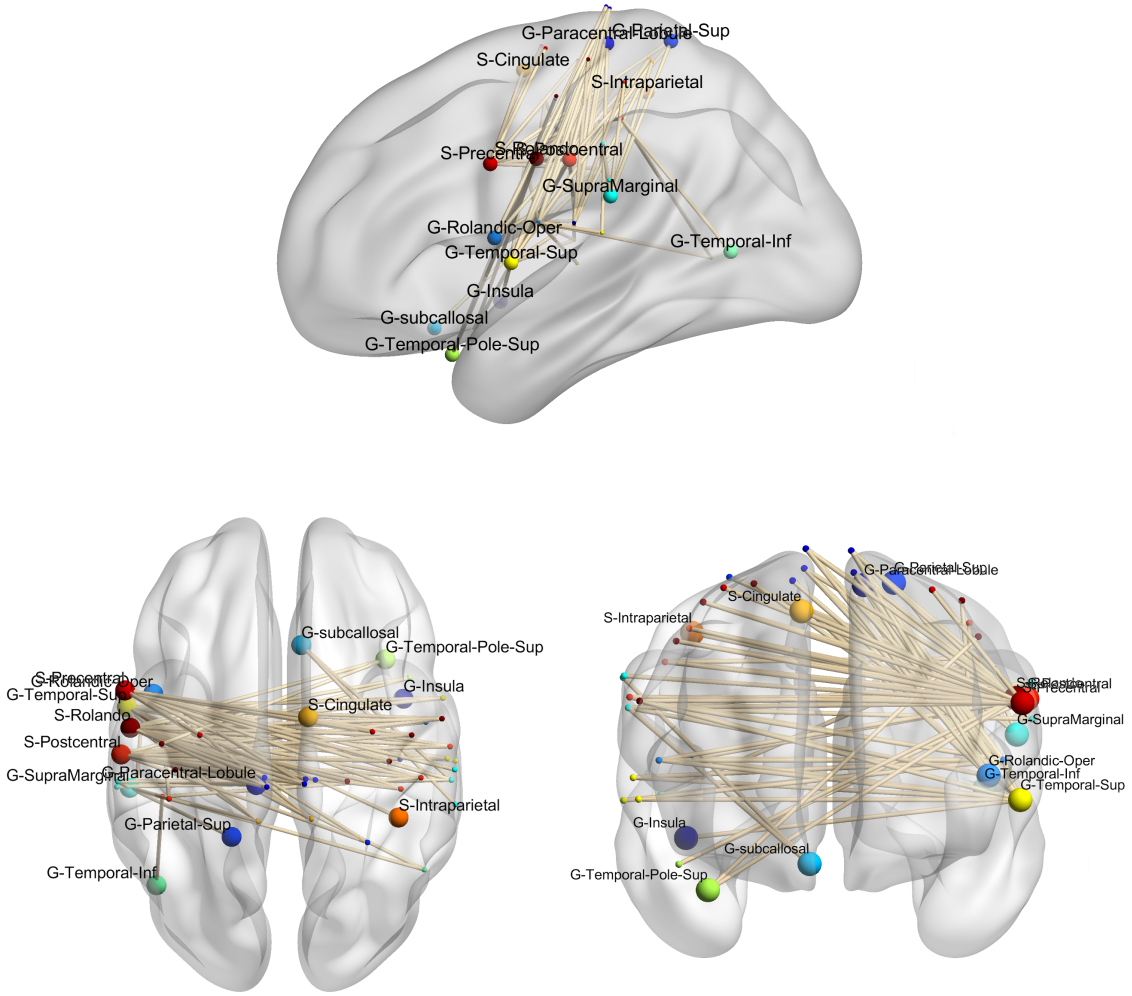

Figure 4.4: Subnetwork identified by the NBS approach with threshold 4.0 in both hemispheres

The same analytic pipeline is applied to normalized correlation coefficients for ROIs on left hemisphere.

The adjacency matrices present in Figure 4.5 show the subnetworks identified by the NBS approach with thresholds $3.0, 3.5, 4.0$ and 4.5, which distinguish the two types of aphasia. With the higher threshold, the size of identified subnetwork is smaller. The detailed figures with region labels are presented by Figures B.5, B.6, B.7 and B.8 in Appendix B. The adjacency matrices present in Figure 4.6 show the edges declared significant by baseline approaches and the subnetwork identified by

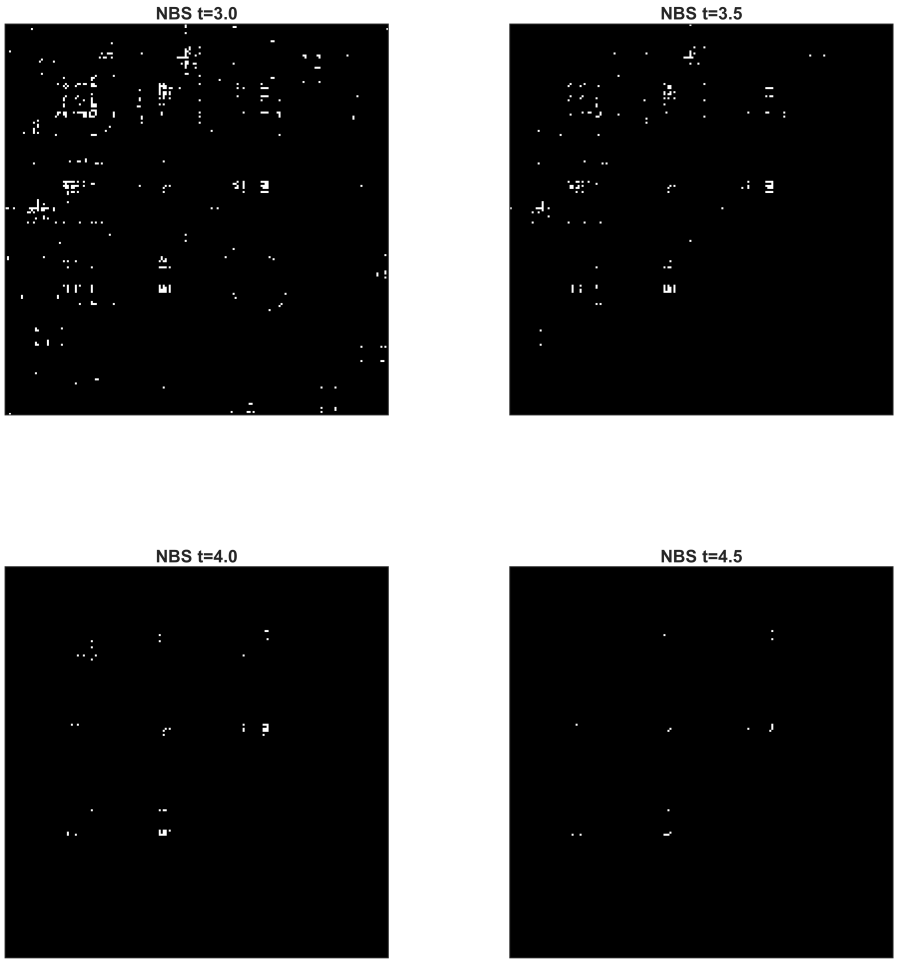

Figure 4.5: Adjacency matrices showing subnetworks identified by the NBS approach with different thresholds

the NBS approach with the threshold 3.0. After comparing the NBS approach with baseline approaches, we find that the results identified by the NBS approach with the threshold 4.0 is similar with the results from baseline approaches.

Figure 4.7 shows the identified subnetwork by the NBS approach with the threshold 3.5 from sagittal plane, axial plane and coronal plane of left hemisphere [Xia, Wang, and He, 2013]. We find the distinctive subnetwork mainly involves ROIs in the premotor, primary motor, prime sensory, Broca's area, parietal cortex and pri-

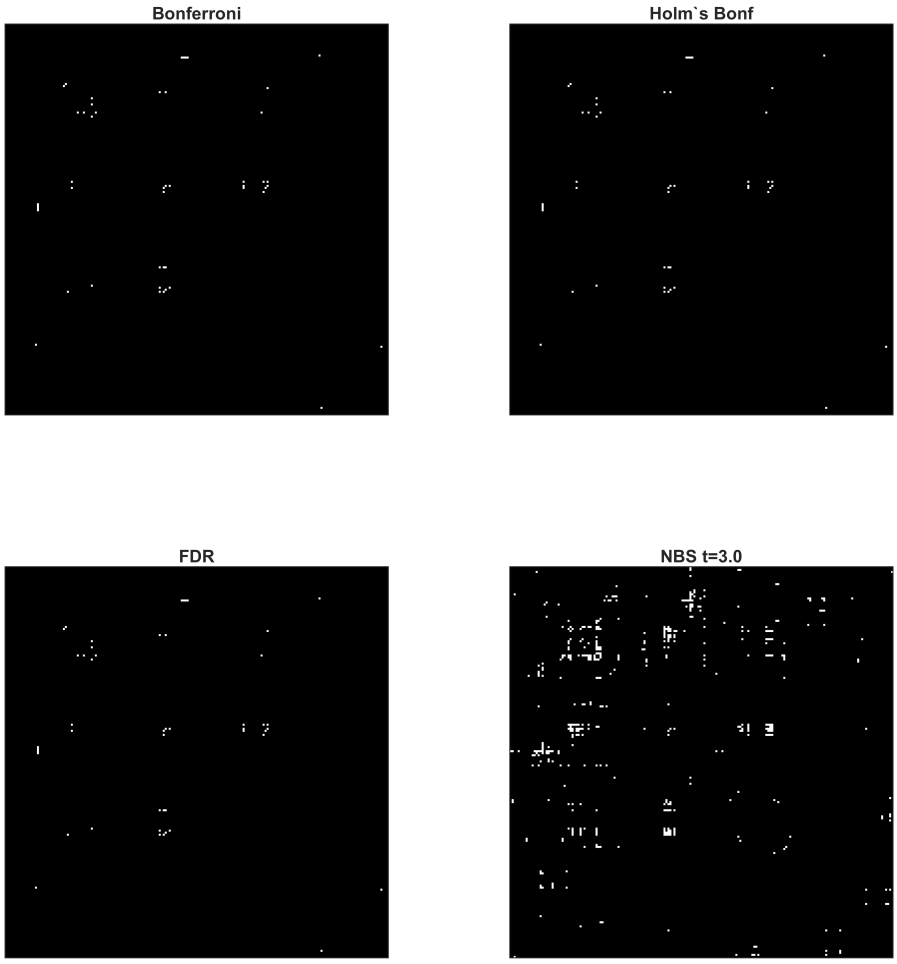

Figure 4.6: Adjacency matrices showing the subnetwork or distinctive edges identified by the NBS and baseline approaches

mary auditory of left hemisphere. These areas are involved in the auditory system and motor system, Table B.2 in Appendix B lists the nodes comprising the subnetwork in left hemisphere and their MNI brain coordinates.

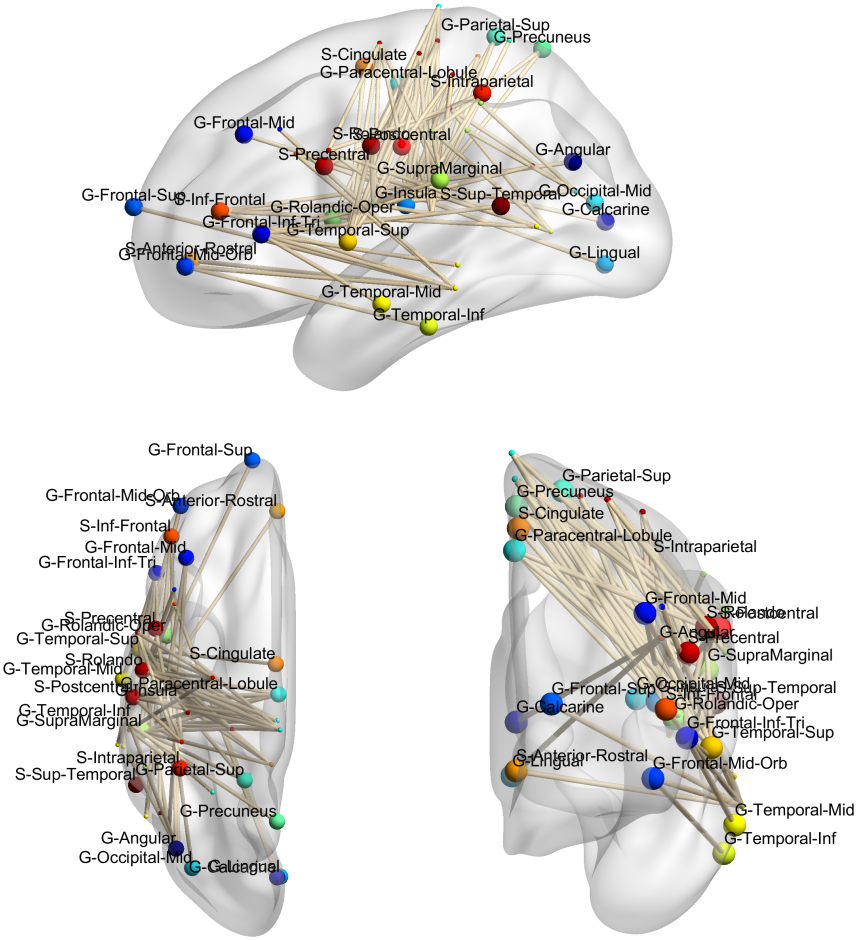

Figure 4.7: Subnetwork identified by the NBS approach with threshold 3.5 in left hemisphere

4.3 Network properties

In this section, we aim to analyze network properties of the distinctive subnetworks, which are identified by the NBS approach with the threshold 4 in both hemispheres and the threshold = 3.5 in left hemisphere. We compute clustering coefficient, degree, and betweenness centrality of the nodes in the subnetworks. Figure 4.8, 4.9 and 4.10 show the histograms of clustering coefficient, degree, and betweenness centrality for the subnetwork identified by the NBS approach in both hemispheres. Figure 4.11 4.12, 4.13 show the histograms of these network measures for the subnetowork in left hemisphere.

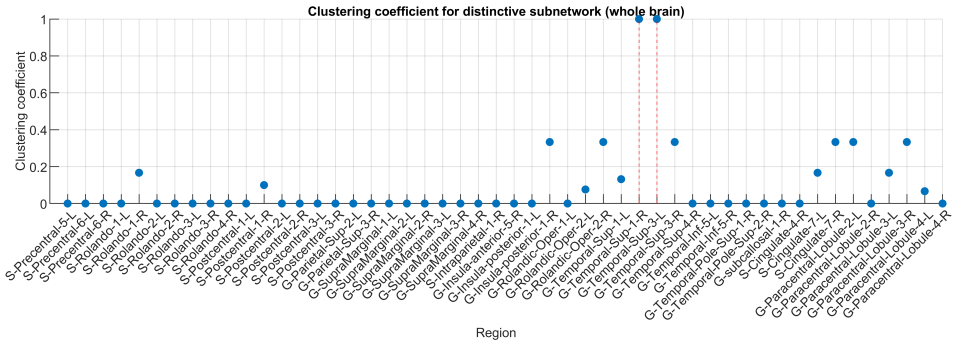

Figure 4.8: Clustering coefficients of the subnetwork in both hemispheres

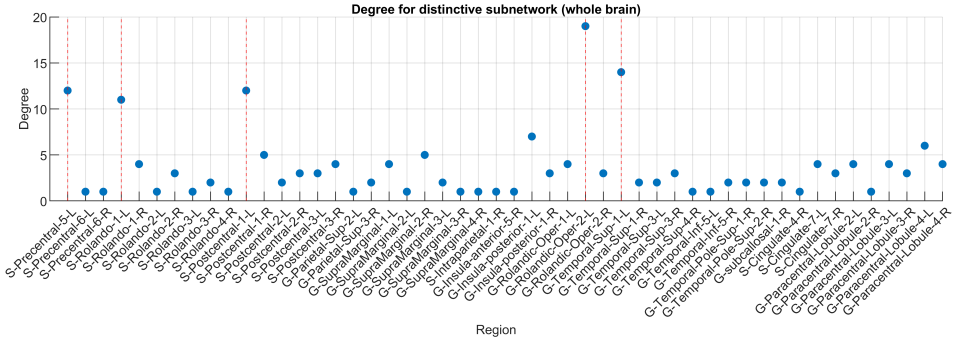

Figure 4.9: Degrees of the subnetwork in both hemispheres

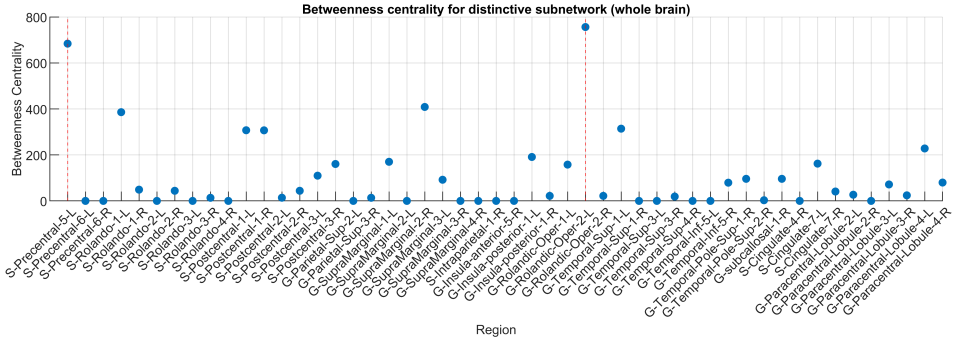

Figure 4.10: Betweenness centrality of the subnetwork in both hemispheres

From the histograms of the distinctive subnetwork in both hemispheres, we find the nodes in right premotor cortex and left primary sensory cortex have very large clustering coefficients. This indicates there are intensive interactions around the premotor cortex and primary sensory cortex. In addition, the nodes in left premotor cortex, left primary auditory cortex and primary motor cortex have high degrees. The degrees of nodes in the premotor cortex indicates there are more than 10 edges in the

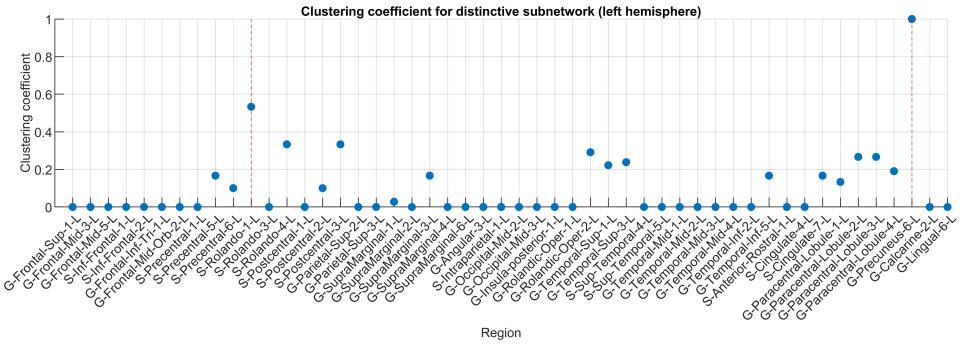

Figure 4.11: Clustering coefficients of the subnetwork in left hemisphere

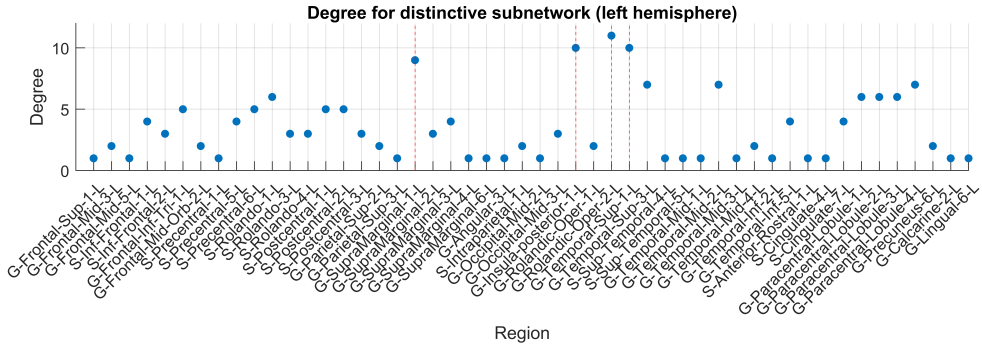

Figure 4.12: Degrees of the subnetwork in left hemisphere

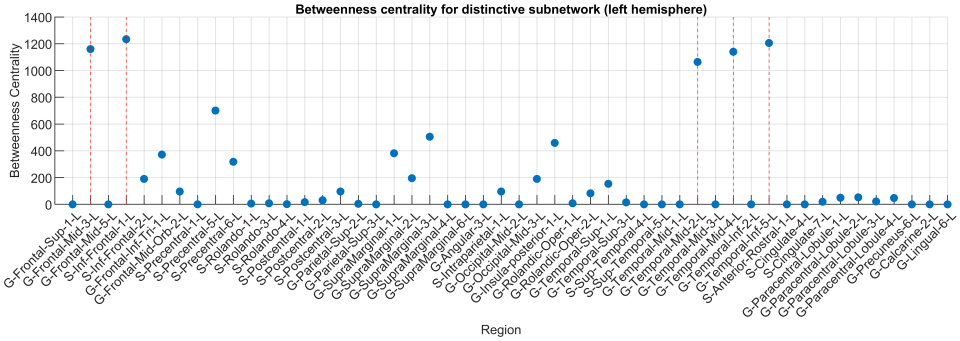

Figure 4.13: Betweenness centrality of the subnetwork in left hemisphere

subnetwork are connected to them. The nodes in left premotor cortex, left primary motor cortex exhibit high betweenness centrality. This indicates these two cortices play an important role in information flow and overall communication efficiency in the subnetwork that distinguishes the two types of aphasia.

For the subnetwork in left hemisphere, besides left premotor, we find the clustering coefficient of the node in left secondary sensorimotor is very large. This means there

exists a clustered organization around left secondary sensorimotor which is different between two types of aphasia. From the measures of centrality, we find the degrees of nodes in the primary motor, primary auditory cortex, and supramarginal gyrus are much larger than others. This indicates there are a large number of edges connected to these nodes. When we look at the betweenness centrality, the nodes in dorsolateral prefront cortex and temporal area have a large value. This indicates the dorsolateral prefront cortex and temporal area comprise the bridge that connects to the other regions in the subnetwork.

Chapter 5

Conclusion

This thesis identifies a functional subnetwork that distinguishes anomic and Broca's aphasia through the NBS approach. The subnetwork is located in the premotor, primary motor, primary auditory and prime sensory cortex. Furthermore, based on the complex network measures, the nodes that are located at the left premotor cortex show intensive interaction and high centrality in this subnetwork.

In comparison with the baseline approaches, the NBS approach controls the FWER at a component level. If the suprathreshold edges form a subnetwork or conected component, the NBS approach can offer substantially greater power [Zalesky, Fornito, and Bullmore, 2010]. However, if suprathreshold edges are isolated and cannot form a connected component, then the NBS approach would fail to make any decision. Another key factor that affects component size and determines whether suprathreshold edges can form a connected component is the threshold in NBS approach. The threshold selection problem will be addressed in a future study. The methods will also be applied to other types of aphasia for a better understanding of the neural processing streams from a network perspective.

Bibliography

Ahuja, R., T. L. Magnanti, J. B. Orlin, and M. R. Reddy (1993). "Network flows:theory algorithms and applications". In: Prentice Hall.

Ashby, F. G. (2011). "Introduction". In: *Statistical Analysis of fMRI data*. Cambridge, MA: The MIT Press. Chap. 1, p. 3.

Benjamini, Y. and Y. Hochberg (1995). "Controlling the False Discovery Rate: A Practical and Powerful Approach to Multiple Testing". In: *Journal of the Royal Statistical Society. Series B (Methodological)* 57 (1), pp. 289–300.

Benjamini, Yoav and Daniel Yekutieli (2001). "The control of the false discovery rate in multiple testing under dependency". In: *Ann. Statist.* 29.4, pp. 1165–1188. DOI: 10.1214/aos/1013699998. URL: https://doi.org/10.1214/aos/1013699998.

Bonferroni, C.E (1936). "Teoria statistica delle classi e calcolo delle probabilità". In: *Pubblicazioni del R Istituto Superiore di Scienze Economiche e Commerciali di Firenze*.

Dronkers, N.F. and J.V. Baldo (2009). "Language: Aphasia". In: *Encyclopedia of Neuroscience*. Ed. by R. L. Squire. Oxford: Academic Press, pp. 343–348.

Erdős, P. and A. Rényi (1960). "On the evolution of random graphs". In: *Mathematical Institute of the Hungarian Academy of Sciences* 5, 17–61.

Farahani, V. F., W. Karwowski, and R. N. Lighthall (2019). "Application of Graph Theory for Identifying Connectivity Patterns in Human Brain Networks: A Systematic Review". In: *Frontiers in Neuroscience* 13. DOI: https://doi.org/10.3389/fnins.2019.00585.

Fisher, A. R. (1915). "Frequency Distribution of the Values of the Correlation Coefficient in Samples from an Indefinitely Large Population". In: *Biometrika* 10(4), 507–521. DOI: https://doi.org/10.2307/2331838.

Freeman, L. (1977). "A Set of Measures of Centrality Based on Betweenness". In: *Sociometry* 40(1), pp. 35–41. DOI: https://doi.org/10.2307/3033543.

Hickok, G., U. Bellugi, and E. S. Klima (1998). "The neural organization of language: evidence from sign language aphasia". In: *Trends in cognitive sciences* 2(4), pp. 129–136. DOI: https://doi.org/10.1016/s1364-6613(98)01154-1.

Hickok, G., J. Houde, and F. Rong (2011). "Sensorimotor integration in speech processing: computational basis and neural organization". In: *Neuron* 69(3), pp. 407–422. DOI: https://doi.org/10.1016/j.neuron.2011.01.019.

Holm, S. (1979). "A Simple Sequentially Rejective Multiple Test Procedure". In: *Scandinavian Journal of Statistics* 6(2), pp. 65–70. URL: http://www.jstor.org/stable/4615733.

Joliot, M., G. Jobard, N. Naveau M.and Delcroix, L. Petit, L. Zago, F. Crivello, E. Mellet, B. Mazoyer, and N. Tzourio-Mazoyer (2015). "AICHA: An atlas of intrinsic connectivity of homotopic areas". In: *Journal of neuroscience methods* 254. DOI: https://doi.org/10.1016/j.jneumeth.2015.07.013.

Kertesz, A. and E. Poole (2004). "The aphasia quotient: the taxonomic approach to measurement of aphasic disability.1974". In: *The Canadian journal of neurological sciences. Le journal canadien des sciences neurologiques* 31(2), pp. 175–184. DOI: https://doi.org/10.1017/s0317167100120736.

Lindquist, M. A. (2008). "The Statistical Analysis of fMRI Data". In: *Statistical Science* 23(4), pp. 439–464. DOI: https://doi.org/10.1214/09-STS282.

Meghanathan, N. (2016). "A computationally lightweight and localized centrality metric in lieu of betweenness centrality for complex network analysis". In: *Vietnam Journal of Computer Science* 4, pp. 23–38. DOI: https://doi.org/10.1007/s40595-016-0073-1.

Ogawa, S., D. W. Tank, R. Menon, J. M. Ellermann, S. G. Kim, H. Merkle, and K. Ugurbil (1992). "Intrinsic signal changes accompanying sensory stimulation: Functional brain mapping with magnetic resonance imaging". In: *Proceedings of the National Academy of Sciences of the United States of America* 89(13), pp. 5951–5955. DOI: https://doi.org/10.1073/pnas.89.13.5951.

Rogers, B. P., V. L. Morgan, A.T. Newton, and J.C Gore (2001). "Assessing functional connectivity in the human brain by fMRI". In: *Magnetic resonance imaging* 25(10), pp. 1347–1357. DOI: https://doi.org/10.1016/j.mri.2007.03.007.

Rubinov, M. and O. Sporns (2010). "Complex network measures of brain connectivity: Uses and interpretations". In: *NeuroImage* 52(3), pp. 1059–1069. DOI: https://doi.org/10.1016/j.neuroimage.2009.10.003.

Van den Heuvel, P. M. and E. H. Hulshoff Pol (2010). "Exploring the brain network: A review on resting-state fMRI functional connectivity". In: *European Neuropsychopharmacology* 20(8). DOI: https://doi.org/10.1016/j.euroneuro.2010.03.008.

Van den Heuvel, P. M. and O. Sporns (2013). "Network hubs in the human brain". In: *Trends in Cognitive Sciences* 17(12), pp. 683 –696. DOI: https://doi.org/10.1016/j.tics.2013.09.012.

Watts, J. D. and S.H. Strogatz (1998). "Collective dynamics of 'small-world' networks". In: *Nature* 393, pp. 440–442. DOI: https://doi.org/10.1038/30918.

Wen, T. and S. Hsieh (2016). "Network-Based Analysis Reveals Functional Connectivity Related to Internet Addiction Tendency". In: *Frontiers in Human Neuroscience* 10, p. 6. DOI: https://doi.org/10.1109/10.3389/fnhum.2016.00006.

Xia, M., J. Wang, and Y. He (2013). "BrainNet Viewer: A Network Visualization Tool for Human Brain Connectomics". In: *PLOS ONE* 8(7), pp. 1–15. DOI: https://10.1371/journal.pone.0068910.

Xu, T., R.K. Cullen, B. Mueller, W. M Schreiner, Lim O. K., S. C. Schulz, and k. k. Parhi (2016). "Network analysis of functional brain connectivity in borderline personality disorder using resting-state fMRI". In: *NeuroImage: Clinical* 11, pp. 302 –315. DOI: https://doi.org/10.1016/j.nicl.2016.02.006.

Yourganov, G., J. Fridriksson, B. Stark, and C. Rorden (2017). "Removal of artifacts from resting-state fMRI data in stroke". In: *NeuroImage. Clinical* 17, 297–305. DOI: https://doi.org/10.1016/j.nicl.2017.10.027.

Zalesky, A., A. Fornito, and T. E. Bullmore (2010). "Network-based statistic: Identifying differences in brain networks". In: *NeuroImage* 53(4), pp. 1197 –1207. DOI: https://doi.org/10.1016/j.neuroimage.2010.06.041.

Zhan, Y., H. Yao, P. Wang, B. Zhou, Z. Zhang, Y. Guo, N. An, J. Ma, X. Zhang, and Y. Liu (2016). "Network-Based Statistic Show Aberrant Functional Connectivity in Alzheimer's Disease". In: *IEEE Journal of Selected Topics in Signal Processing* 10(7), pp. 1182–1188. DOI: https://doi.org/10.1109/JSTSP.2016.2600298.

Appendix A

Theorem Proof of FWER controlling

A.1 NBS approach

Let H_0 denote the case where the null hypothesis is true for each edge. Suppose the size of connected component i is s_i and size of connected component after applying a threshold is t_α. By definition of the FWE rate, it follows that

$$\begin{aligned}
\text{FWER} &= P\left(1 \text{ or more components declared significant } |H_0\right) \\
&= 1 - P\left(\text{ no components declared significant } |H_0\right) \\
&= 1 - P\left(\bigcup_i \{s_i \leq t_\alpha\} | H_0\right) \\
&= 1 - P\left(\max_i \{s_i\} \leq t_\alpha\} | H_0\right) \\
&= \alpha\,.
\end{aligned}$$

A.2 Bonferrioni correction

Suppose we have m hypotheses. In addition, $p_1, \ldots, p_m$ are their corresponding p-values. The Bonferroni correction rejects the null hypothesis for each $p_i \leq \frac{\alpha}{m}$, $i = 1, 2 \ldots m$, thereby controlling the FWE rate at α. The proof of this control is the direct application of Boole's inequality, as follows

$$\text{FWER} = P\left\{\bigcup_{i=1}^{m_0}\left(p_i \leq \frac{\alpha}{m}\right)\right\} \leq \sum_{i=1}^{m_0}\left\{P\left(p_i \leq \frac{\alpha}{m}\right)\right\} = m_0\frac{\alpha}{m} \leq m\frac{\alpha}{m} = \alpha\,,$$

m_0 is the number of true null hypotheses and $m_0 < m$. This control does not require any assumptions about dependence among the p-values or about how many of the

null hypotheses are true. If decisions of hypotheses are all independent or disjoint events, then the inequality becomes an equality according to the Kolmogorov Axioms.

A.3 Holm's Bonfeeroni correction

Suppose we have m separate hypotheses, $H^{(1)}, H^{(2)} \dots H^{(m)}$ and their corresponded p-values are sorted: $p_{(1)}, p_{(2)} \dots p_{(m)}$. Let I_0 be the set of indices of true null hypotheses and m_0 is the number of elements in I_0.

Let k be the first rejected true hypothesis and $H^{(1)}, H^{(2)} \dots H^{(k-1)}$ are reject false hypotheses, where $k - 1 \leq m - m_0$. Then we get

$$\frac{1}{m-k+1} \leq \frac{1}{m_0}\,. \tag{A.1}$$

Since k is rejected, we have $p_{(k)} \leq \frac{\alpha}{m-k+1}$ by definition of test. By inequality $A.1$, thus, if we wrongly reject a true hypothesis, there has to be a true hypothesis with p-value at most $\frac{\alpha}{m_0}$.

Therefore, by Boole's inequality,

$$\text{FWER} = P\left(p_i < \frac{\alpha}{m_0}, \text{for } i \in I_0\right) \leq \sum_{i \in I_0} P\left(p_i < \frac{\alpha}{m_0}\right) = m_0 \frac{\alpha}{m_0} = \alpha\,.$$

In addition, this control also does not require any assumptions about dependence among the p-values or about how many of the null hypotheses are true. If decisions of hypotheses are all independent, then the inequality becomes an equality according to the Kolmogorov Axioms.

A.4 FDR control (BH step-up procedure)

FDR-controlling procedures are designed to control the expected proportion of false discoveries rate at q instead of FWER. Suppose we have m separate hypotheses, $H^{(1)}, H^{(2)} \dots H^{(m)}$ and their corresponded independent p-values are sorted: $p_{(1)}, p_{(2)} \dots p_{(m)}$. Let $0 \leq m_0 \leq m$ independent p-values corresponding to true null

hypotheses, and for $m_1 = m - m_0$ p-values corresponding to the false null hypotheses. Finally, define j_0 to be the largest index satisfying,

$$p_j \leq \frac{m_0 + j}{m+1} q,$$

with $0 \leq j \leq m_1$ and denote the right-side of inequality by p''.

Let $\mathbf{Q}$ be the FDR, then

$$\begin{aligned} E(\mathbf{Q}|p_{(m_0+1)}, p_{(m_0+2)} \dots p_{(m)}) = &\int_0^{p''} E\left(\mathbf{Q}|p_{(m_0+1)}, p_{(m_0+2)} \dots p_{(m)}\right) f'_{p_{(m_0)}}(p)\mathrm{d}p \\ &+ \int_{p''}^1 E\left(\mathbf{Q}|p_{(m_0+1)}, p_{(m_0+2)} \dots p_{(m)}\right) f_{p'_{(m_0)}}(p)\mathrm{d}p\,. \end{aligned} \tag{A.2}$$

In the first part, all hypotheses are rejected and $\mathbf{Q} \equiv \frac{m_0}{m_0+j_0}$, we obtain

$$\frac{m_0}{m_0+j_0}\left(p''\right)^{m_0} \leq \frac{m_0}{m_0+j_0}\frac{m_0+j_0}{m+1} q \left(p''\right)^{m_0-1} = \frac{m_0}{m+1} q \left(p''\right)^{m_0-1}. \tag{A.3}$$

By the definition of test, we know a hypothesis $H^{(i)}$ can be rejected if there exists k, $i \leq k \leq m_0 + j - 1$, for which $p_{(k)} \leq [k/(m+1)]q$, or equivalently

$$\frac{p_{(k)}}{p} \leq \frac{k}{m_0+j-1}\frac{m_0+j-1}{(m+1)p} q\,, \tag{A.4}$$

where $p_{(m_0)} = p$.

Using inequality $A.4$, we have

$$E\left(\mathbf{Q}|p_{(m_0+1)}, p_{(m_0+2)} \dots p_{(m)}\right) \leq \frac{m_0-1}{m_0+j-1}\frac{m_0+j-1}{(m+1)p} q = \frac{m_0-1}{(m+1)p} q \tag{A.5}$$

The bound in inequality $A.5$ depends on p, not on $p_{(m_0+1)} \dots p_m$, so the second part

$$\begin{aligned} \int_{p''}^1 E\left(\mathbf{Q}|p_{(m_0+1)}, p_{(m_0+2)} \dots p_{(m)}\right) f'_{P_{(m_0)}}(p)\mathrm{d}p &\leq \int_{p''}^1 \frac{m_0-1}{(m+1)p} q m_0 p^{(m_0-1)}\mathrm{d}p \\ = \frac{m_0}{m+1} q \int_{p''}^1 (m_0-1)\, p^{(m_0-2)}\mathrm{d}p &= \frac{m_0}{m+1} q \left[1 - p''\,(m_0-1)\right]. \end{aligned} \tag{A.6}$$

Adding inequality $A.3$ and $A.6$, we have

$$E\left(\mathbf{Q}|p_{(m_0+1)}, p_{(m_0+2)} \dots p_{(m)}\right) \leq \frac{m_0}{m} q\,.$$

In addition, since $m_1 = m - m_0$ of hypotheses are false, integrating inequality above, we obtain

$$E(\mathbf{Q}) \leq \frac{m_0}{m} q \leq q$$

and FDR is controlled.

The BH procedure is valid when the m tests are independent, and also when tests are positive dependent, but is not universally valid [Benjamini and Yekutieli, 2001].

Appendix B

Subnetworks identified by NBS approach

B.1 Results for both hemispheres

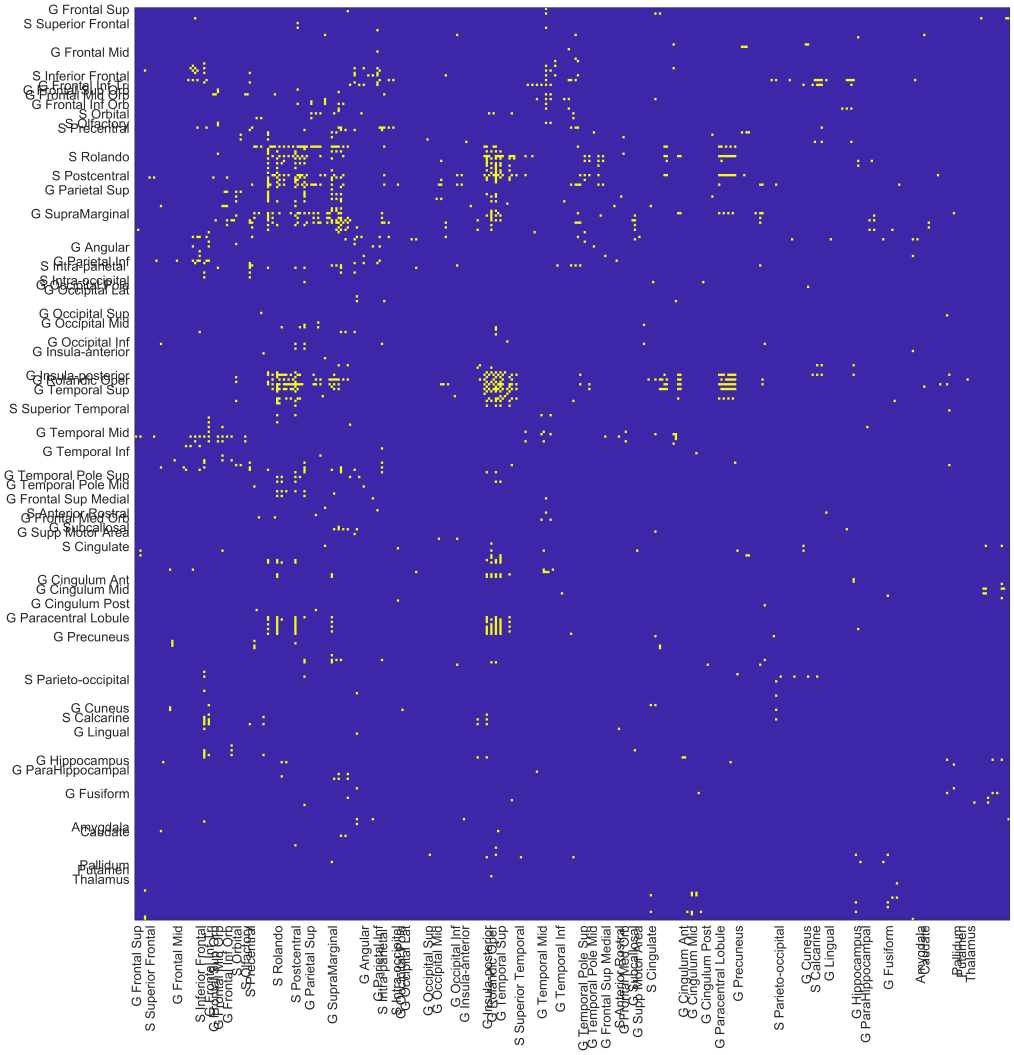

Figure B.1: Adjacency matrix showing the subnetwork identified by the NBS approach with the threshold 3.0

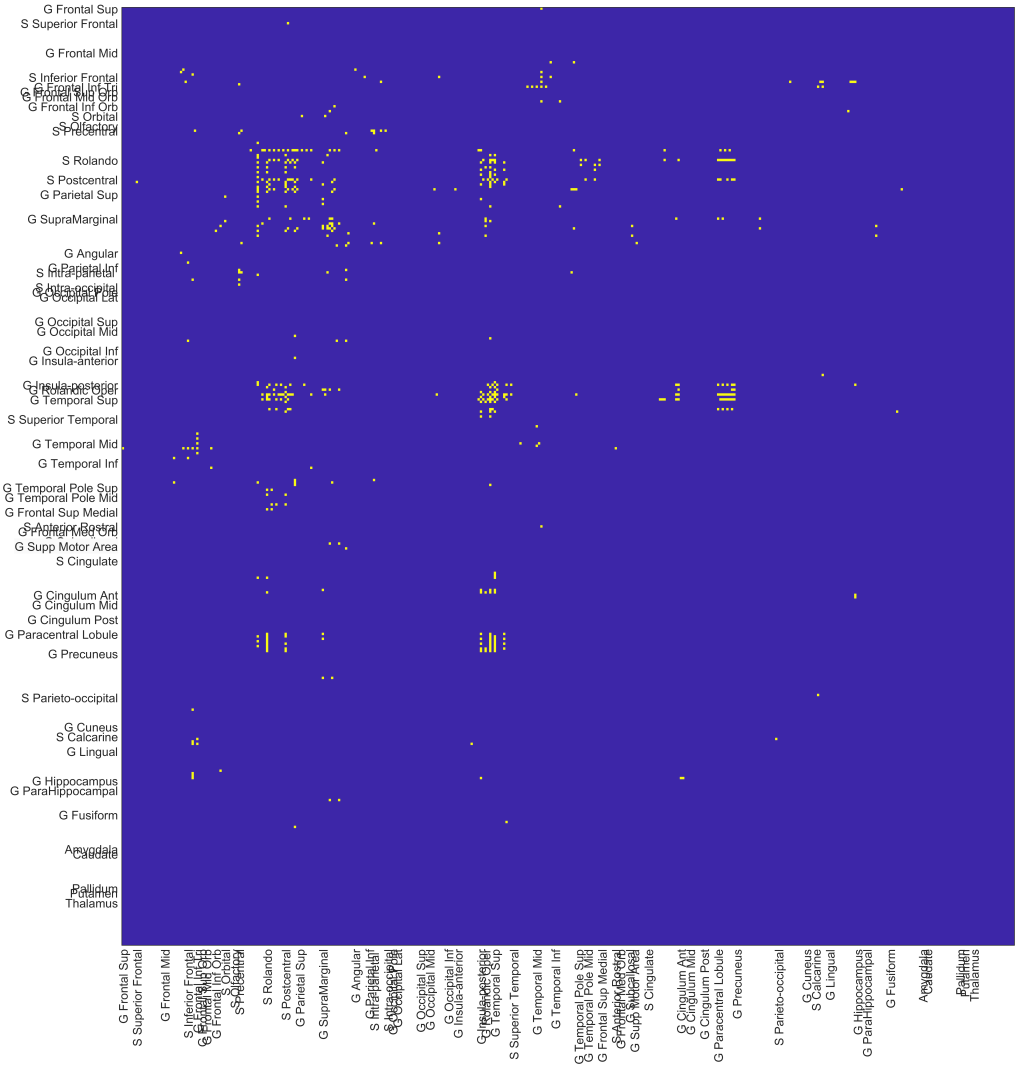

Figure B.2: Adjacency matrix showing the subnetwork identified by the NBS approach with the threshold 3.5

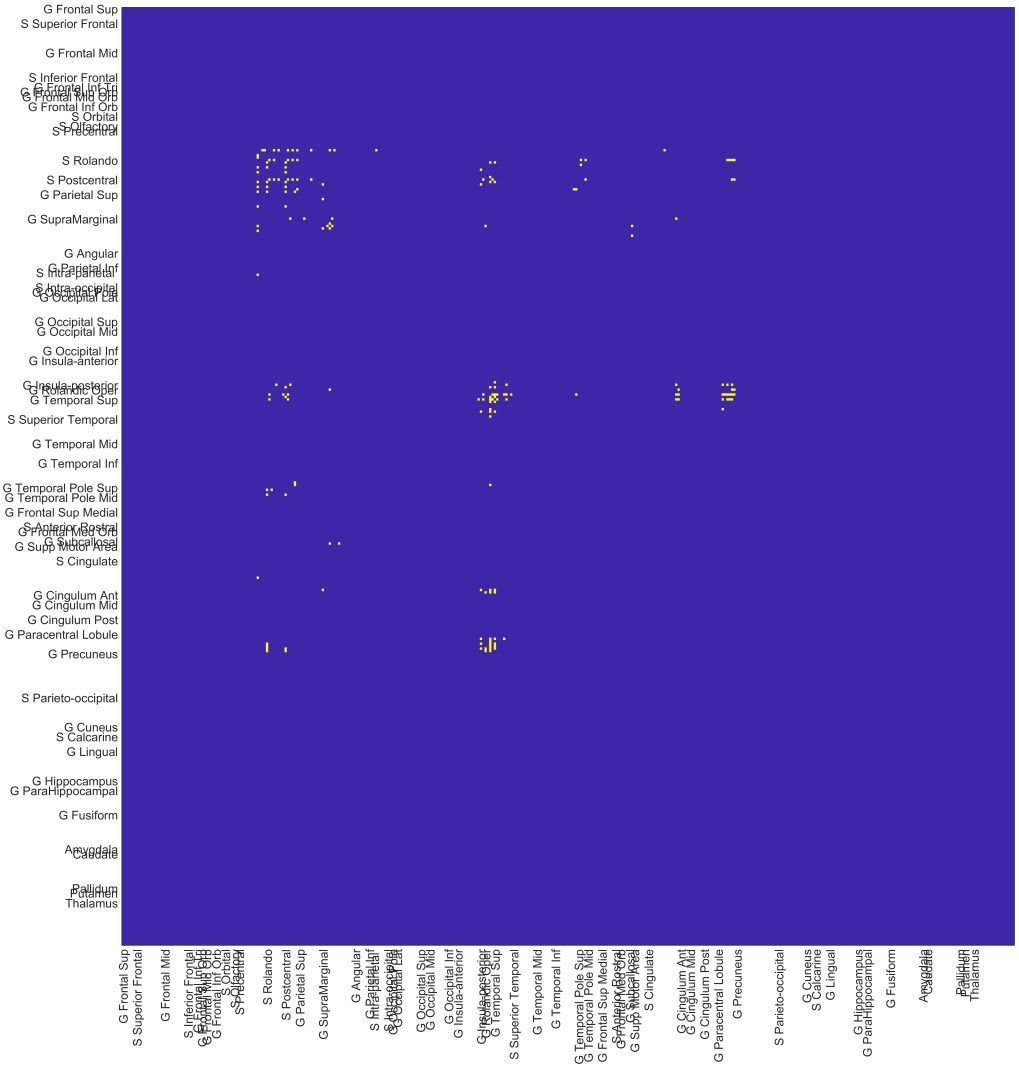

Figure B.3: Adjacency matrix showing the subnetwork identified by the NBS approach with the threshold 4.0

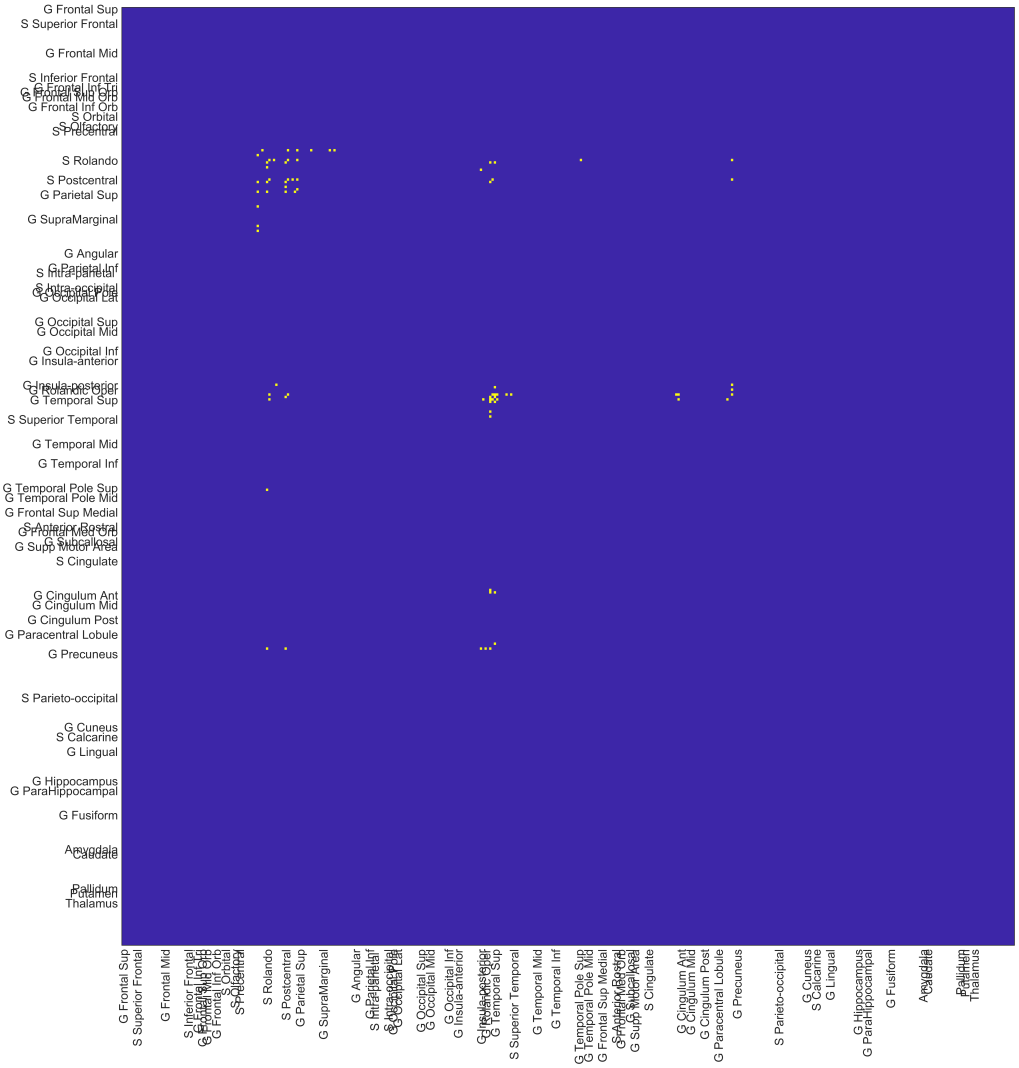

Figure B.4: Adjacency matrix showing the subnetwork identified by the NBS approach with the threshold 4.5

Table B.1: Identified subnetwork through the NBS approach with the threshold 4.0 in both hemispheres

Node	**MNI Coordinates**
S-Precentral-5-L	(-56.11,4.79,30.58)
S-Precentral-6-L	(-29.82,-10.98,63.59)
S-Precentral-6-R	(30.91,-9.8,64.17)
S-Rolando-1-L	(-54.26,-8.37,31.99)
S-Rolando-1-R	(55.4,-5.2,31.14)
S-Rolando-2-L	(-43.23,-14.04,49.93)
S-Rolando-2-R	(44.72,-10.92,48.62)
S-Rolando-3-L	(-38.47,-23.15,60.43)
S-Rolando-3-R	(36.85,-20.19,59.98)
S-Rolando-4-R	(22.09,-27.27,65.36)
S-Postcentral-1-L	(-57.52,-17.78,31.75)
S-Postcentral-1-R	(58.27,-15,32.29)
S-Postcentral-2-L	(-40.65,-33.42,53.87)
S-Postcentral-2-R	(40.89,-29.91,52.31)
S-Postcentral-3-L	(-43.06,-32.64,43.56)
S-Postcentral-3-R	(47.97,-25.97,42.54)
G-Parietal-Sup-2-L	(-18.66,-46.78,65.65)
G-Parietal-Sup-3-R	(29.22,-48.76,67.22)
G-SupraMarginal-1-L	(-54.47,-29.51,21.37)
G-SupraMarginal-2-L	(-58.95,-29.15,25.89)
G-SupraMarginal-2-R	(58.72,-26.76,29.19)
G-SupraMarginal-3-L	(-58.68,-27.33,36.33)
G-SupraMarginal-3-R	(59.86,-23.09,38.5)
G-SupraMarginal-4-R	(60.16,-35.41,38.01)

S-Intraparietal-1-R	(40.1,-40,51)
G-Insula-anterior-5-R	(41.85,1.86,-8.75)
G-Insula-posterior-1-L	(-42.08,-19.1,13.71)
G-Insula-posterior-1-R	(40.61,-19.46,14.31)
G-Rolandic-Oper-1-L	(-46.26,3.59,9.39)
G-Rolandic-Oper-2-L	(-50.59,-8.96,13.91)
G-Rolandic-Oper-2-R	(49.74,-6.32,13.89)
G-Temporal-Sup-1-L	(-55.47,-1.12,2.3)
G-Temporal-Sup-1-R	(55.71,2.1,2.53)
G-Temporal-Sup-3-L	(-52,-27.13,10.92)
G-Temporal-Sup-3-R	(57.27,-19.18,8.83)
G-Temporal-Sup-4-R	(60.05,-19.98,2.2)
G-Temporal-Inf-5-L	(-45.09,-63.82,5.5)
G-Temporal-Inf-5-R	(49.22,-58.33,3.81)
G-Temporal-Pole-Sup-1-R	(35.51,15.7,-23.94)
G-Temporal-Pole-Sup-2-R	(43.98,9.24,-16.45)
G-subcallosal-1-R	(5.89,20.74,-16.33)
S-Cingulate-4-R	(8.25,-4.64,57.31)
S-Cingulate-7-L	(-9.28,-41.32,59.51)
S-Cingulate-7-R	(9.41,-40.52,60.51)
G-Paracentral-Lobule-2-L	(-9.94,-28.55,64.96)
G-Paracentral-Lobule-2-R	(10.82,-26.75,66.21)
G-Paracentral-Lobule-3-L	(-7.01,-25.89,68.59)
G-Paracentral-Lobule-3-R	(7.43,-26.48,69.8)
G-Paracentral-Lobule-4-L	(-6.26,-29.26,74.98)
G-Paracentral-Lobule-4-R	(6.97,-28.27,75.54)

B.2 Results for left hemisphere

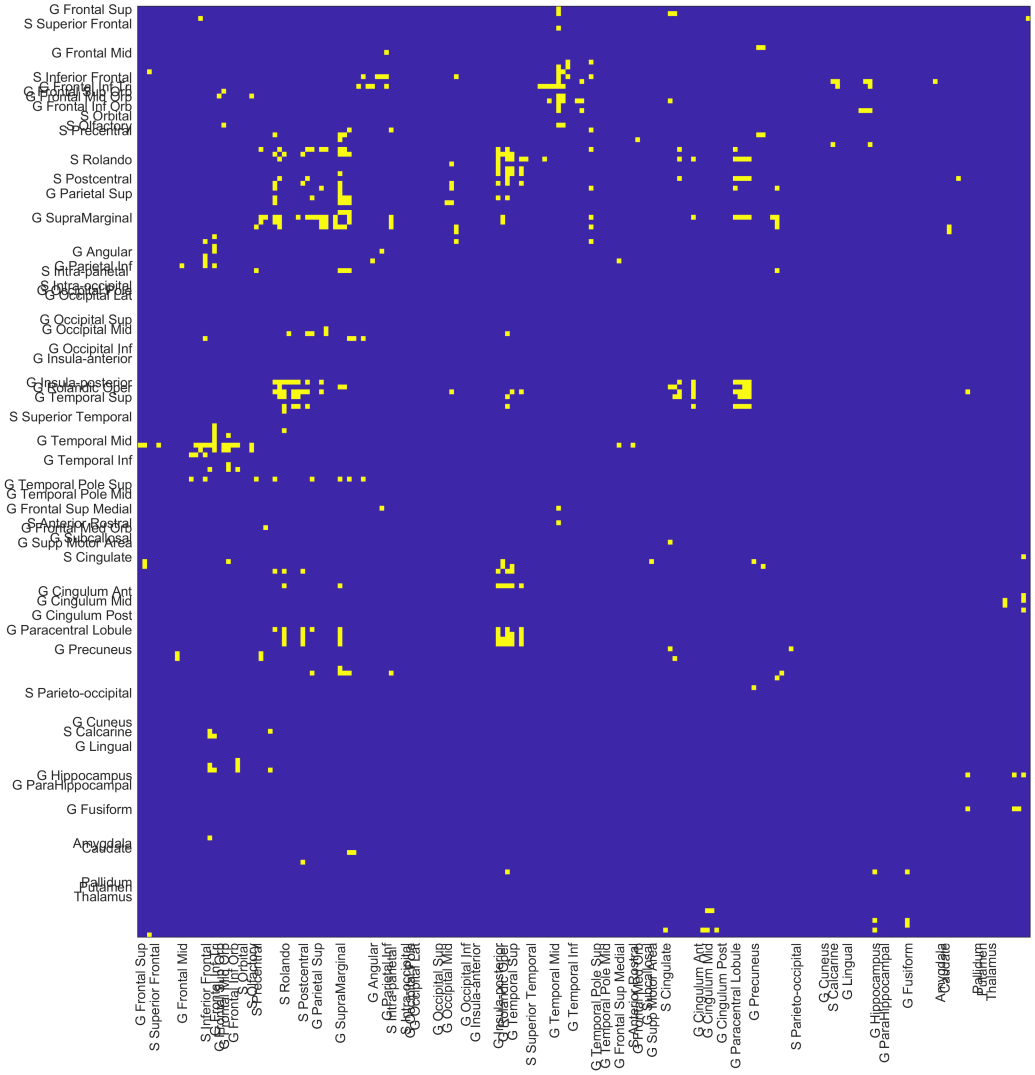

Figure B.5: Adjacency matrix showing the subnetwork identified by the NBS approach with the threshold 3.0

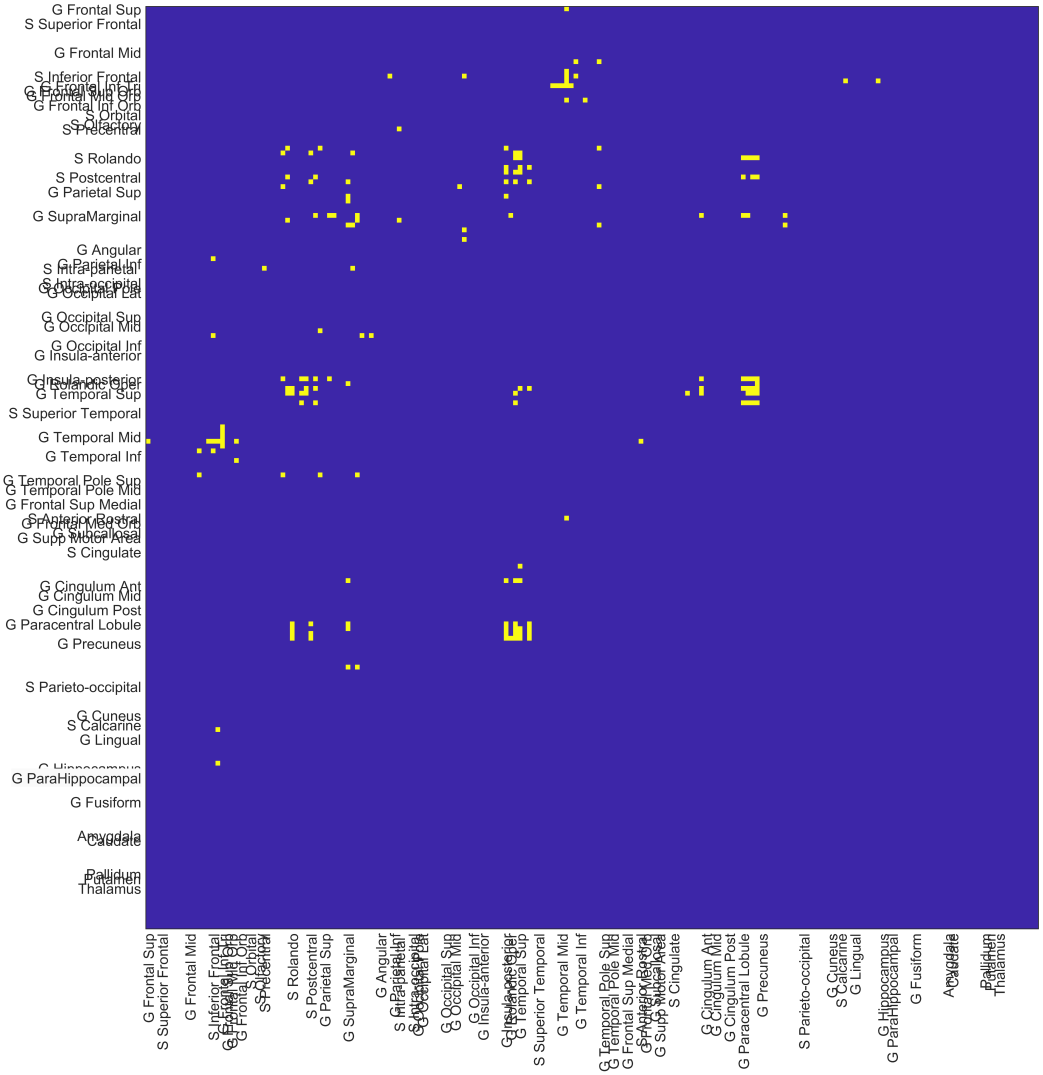

Figure B.6: Adjacency matrix showing the subnetwork identified by the NBS approach with the threshold 3.5

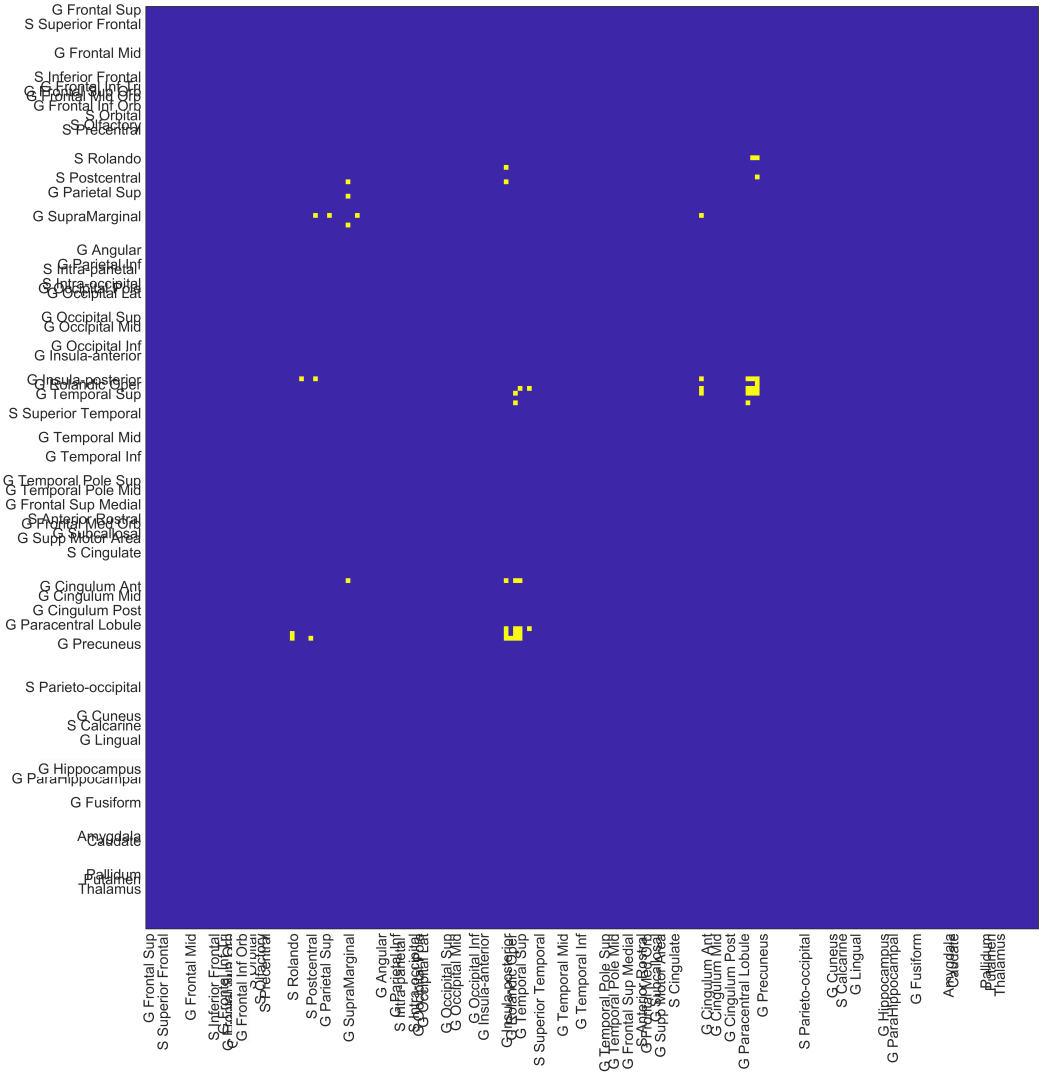

Figure B.7: Adjacency matrix showing the subnetwork identified by the NBS approach with the threshold 4.0

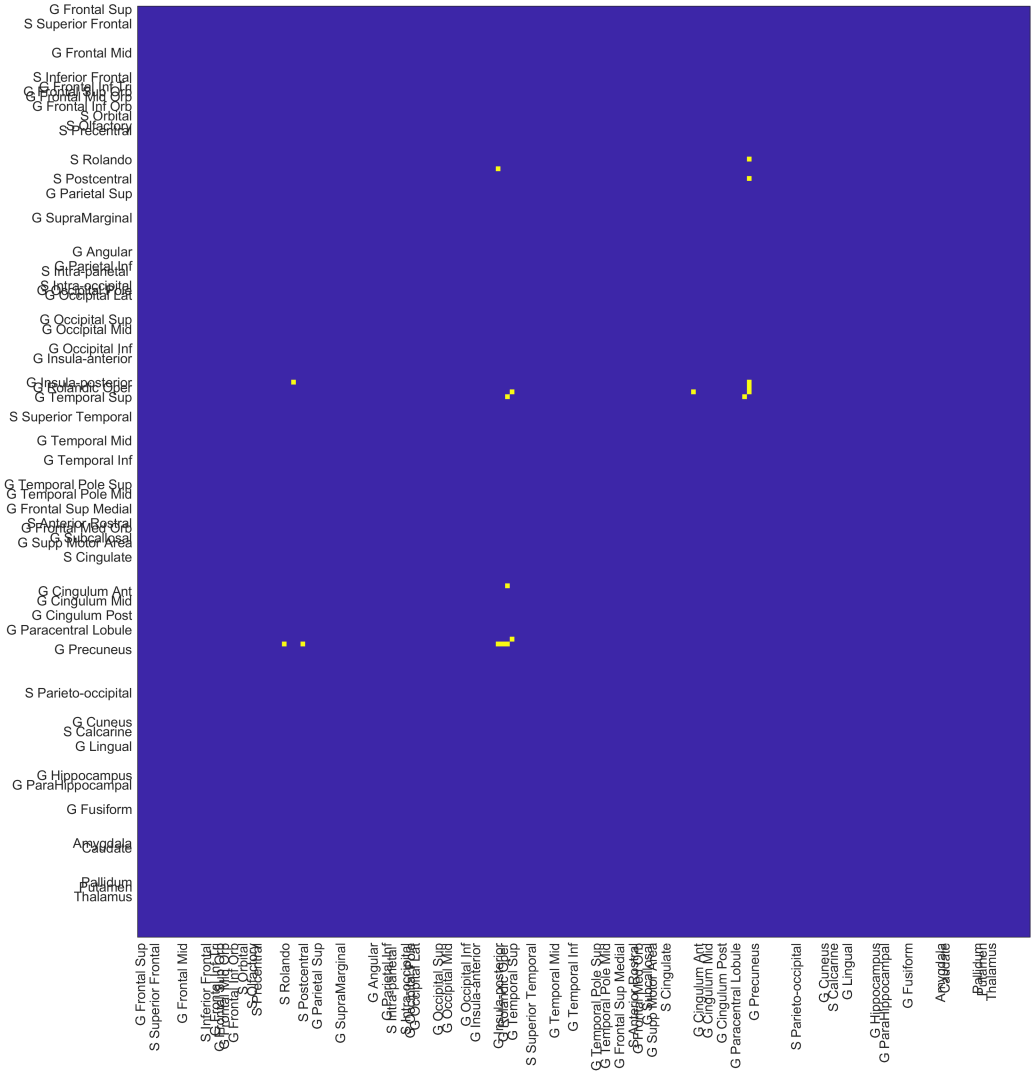

Figure B.8: Adjacency matrix showing the subnetwork identified by the NBS approach with the threshold 4.5

Table B.2: Identified subnetwork through the NBS approach with the threshold 3.5 in left hemisphere

Node	**MNI Coordinates**
G-Frontal-Sup-1-L	(-15.99,64.94,13.08)
G-Frontal-Mid-3-L	(-39.09,30.91,35.44)
G-Frontal-Mid-5-L	(-43.24,19.84,37.07)
S-Inf-Frontal-1-L	(-44.24,38.32,11.74)
S-Inf-Frontal-2-L	(-43.11,14.84,29.41)
G-Frontal-Inf-Tri-1-L	(-49.44,25.56,4.68)
G-Frontal-Mid-Orb-2-L	(-41.05,48.99,-5.31)
S-Precentral-1-L	(-49.74,6.14,25.67)
S-Precentral-5-L	(-56.11,4.79,30.58)
S-Precentral-6-L	(-29.82,-10.98,63.59)
S-Rolando-1-L	(-54.26,-8.37,31.99)
S-Rolando-3-L	(-38.47,-23.15,60.43)
S-Rolando-4-L	(-23.12,-28.85,64.32)
S-Postcentral-1-L	(-57.52,-17.78,31.75)
S-Postcentral-2-L	(-40.65,-33.42,53.87)
S-Postcentral-3-L	(-43.06,-32.64,43.56)
G-Parietal-Sup-2-L	(-18.66,-46.78,65.65)
G-Parietal-Sup-3-L	(-29.87,-50.97,64.37)
G-SupraMarginal-1-L	(-54.47,-29.51,21.37)
G-SupraMarginal-2-L	(-58.95,-29.15,25.89)
G-SupraMarginal-3-L	(-58.68,-27.33,36.33)
G-SupraMarginal-4-L	(-59.13,-37.95,36.67)
G-SupraMarginal-6-L	(-53.46,-42.15,45.1)
G-Angular-3-L	(-42.63,-70.64,27.04)

S-Intraparietal-1-L	(-41.21,-42.62,48.17)
G-Occipital-Mid-2-L	(-36.97,-77.4,14.36)
G-Occipital-Mid-3-L	(-41.73,-71.49,17.95)
G-Insula-posterior-1-L	(-42.08,-19.1,13.71)
G-Rolandic-Oper-1-L	(-46.26,3.59,9.39)
G-Rolandic-Oper-2-L	(-50.59,-8.96,13.91)
G-Temporal-Sup-1-L	(-55.47,-1.12,2.3)
G-Temporal-Sup-3-L	(-52,-27.13,10.92)
S-Sup-Temporal-4-L	(-56.55,-48.37,13.36)
S-Sup-Temporal-5-L	(-48.12,-58.18,25.79)
G-Temporal-Mid-1-L	(-61.21,-11.54,-16.84)
G-Temporal-Mid-2-L	(-62.98,-34.34,-12.07)
G-Temporal-Mid-3-L	(-60.97,-35.03,-4.8)
G-Temporal-Mid-4-L	(-53.09,-59.39,7.03)
G-Temporal-Inf-2-L	(-58.55,-26.07,-23.84)
G-Temporal-Inf-5-L	(-45.09,-63.82,5.5)
S-Anterior-Rostral-1-L	(-7.26,47.2,-3.46)
S-Cingulate-4-L	(-7.81,-6.21,56.39)
S-Cingulate-7-L	(-9.28,-41.32,59.51)
G-Paracentral-Lobule-1-L	(-6.89,-16.76,50.9)
G-Paracentral-Lobule-2-L	(-9.94,-28.55,64.96)
G-Paracentral-Lobule-3-L	(-7.01,-25.89,68.59)
G-Paracentral-Lobule-4-L	(-6.26,-29.26,74.98)
G-Precuneus-6-L	(-7.35,-61.18,61.83)
G-Calcarine-2-L	(-7.3,-80.67,8.59)
G-Lingual-6-L	(-6.26,-80.41,-4.65)